Symmetry Violations in Partially Oxidized One-Dimensional (1D) Transition Metal Polymers. Metal-Ligand-Metal (M-L-M) Bridged Systems

Michael C. Böhm
Max-Planck-Institut für Festkörperforschung, Stuttgart

Z. Naturforsch. **39a**, 807–829 (1984); received June 22, 1984

The band structure of the metal-ligand-metal (M-L-M) bridged quasi one-dimensional (1D) cyclopentadienylmanganese polymer, MnCp **1**, has been studied in the unoxidized state and in a partly oxidized modification with one electron removed from each second MnCp fragment. The tight-binding approach is based on a semiempirical self-consistent-field (SCF) Hartree-Fock (HF) crystal orbital (CO) model of the INDO-type (intermediate neglect of differential overlap) combined with a statistical averaging procedure which has its origin in the grand canonical ensemble. The latter approximation allows for an efficient investigation of violations of the translation symmetries in the oxidized 1D material. The oxidation process in **1** is both ligand- and metal-centered (Mn $3d_{z^2}$ states). The mean-field minimum corresponds to a charge density wave (CDW) solution with inequivalent Mn sites within the employed repeat-units. The symmetry adapted solution with electronically identical 3d centers is a maximum in the variational space. The coupling of this electronic instability to geometrical deformations is also analyzed. The ligand amplitudes encountered in the hole-state wave function prevent extremely large charge separations between the 3d centers which are found in 1D systems without bridging moieties (e.g. $Ni(CN)_4^{2-}$ chain). The symmetry reduction in oxidized **1** is compared with violations of spatial symmetries in finite transition metal derivatives and simple solids. The stabilization of the valence bond-type (VB) solution is physically rationalized (i.e. left-right correlations between the 3d centers). The computational results derived for **1** are generalized to oxidized transition metal chains with band occupancies that are simple fractions of the number of stacking units and to 1D systems that deviate from this relation. The entropy-influence for temperatures $T \neq 0$ is shortly discussed (stabilization of domain or cluster structures).

1. Introduction

The structural, optical, magnetic, chemical and charge carrier properties of low-dimensional materials with organometallic building blocks have been studied extensively in the past decade [1–5]. A large number of systems show semiconducting or highly conducting properties in solids that crystallize in form of segregated stacks (i.e. adjacent donor and acceptor strands). This arrangement often leads to an incomplete charge transfer between the two one-dimensional columns. Different types of stacking patterns are accessible in such systems with 3d, 4d or 5d atoms as central units and a broad spectrum of organic ligands. The one-dimensional (1D) materials can be divided into solids with direct metal-metal contacts (M-M architecture) and 1D chains where the transition metal sites are coupled via bridging ligands (M-L-M type) [6].

The transfer channels and the transport mechanisms of these materials can be modified by changes in the molecular skeletons or counterions. It is possible to discriminate two different carrier paths even in the simplest, highly idealized description: a) 1D stacks with conducting states formed by the spines of the transition metal atoms and b) 1D backbones with charge carriers confined to the diffuse ligand states. Strongly correlated motions of the injected carriers must be expected in the first class of low-dimensional materials as a result of the contracted nature of the nd ($n = 3, 4$) AO's. The physical difference between a) and b) can be illustrated by the operational parameter $U/4t$ measuring the "correlation strength" in infinite Fermion systems in the framework of the simple Hubbard Hamiltonian [7, 8]. U symbolizes the on-site repulsion and $4t$ is the band width (t: hopping integral) of a simple tight-binding band. The strongly correlated regime

Reprint requests to Dr. M. C. Böhm, Max-Planck-Institut für Festkörperforschung, Heisenbergstr. 1, D-7000 Stuttgart 80, West Germany.

0340-4811 / 84 / 0900-0807 $ 01.30/0. – Please order a reprint rather than making your own copy.

(i.e. a)) is defined by $U/4t \rightarrow \infty$ while the diffuse (ligand) regime leads to $U/4t \rightarrow 0$.

The transfer paths a) and b) are only two extremes encountered in the class of extended organometallic chains. On one side, it is possible that the conducting states dispose of significant admixtures from the metal and ligand subspaces; on the other, one has to take into account degeneracies or near-degeneracies between both types of conducting states (doubly mixed valence solids). The rich variety of possible transfer mechanisms in metallomacrocycles has been demonstrated in a series of Ni(II) porphyrinato materials [9–11]. Polaronic transport properties have been detected in 1D chains with large lattice spacings $\tilde{c}$ ($\tilde{c} > 3.75$ Å), $\tilde{c}$ numbers < 3.25 Å lead to band conductivities.

On the basis of measured carrier mobilities μ_C it is often possible to discriminate charge carrier processes a priori into band mechanisms ($\mu_C > 1\,\mathrm{cm}^2\,(\mathrm{Vsec})^{-1}$) and hopping motions between localized states ($\mu_C < 1\,\mathrm{cm}^2\,(\mathrm{Vsec})^{-1}$) [12]. A suitable theoretical tool to investigate the electronic properties of low-dimensional materials belonging to the group of "band conductors" is the crystal orbital (CO) formalism based on the tight-binding approximation [13, 14]. The one-electron states are defined in terms of Bloch orbitals, i.e. the whole crystal is subject to periodic boundary conditions. Most of the CO procedures are defined in the framework of the self-consistent-field (SCF) Hartree-Fock (HF) one-determinantal approximation. Theoretical procedures that lead to improved computational results by taking into account many-body interactions or electron-phonon coupling have been described in the literature [15–17]. Transport processes in narrow-band materials are often discussed in terms of hopping theories [18], polaronic approximations (e.g. small (Holstein) or large (Fröhlich) polarons) [19–21] or percolation models [22, 23] where details of electronic (band) structure calculations are conveniently neglected. Electron-electron or hopping integrals, band widths and gaps, etc. are only adopted as phenomenological parameters that are chosen to fit experimental data.

The preceding discussion touches a central theoretical problem in solid state approaches to partly oxidized (or reduced) low-dimensional materials. It is the question whether hole-states can be represented in terms of spatially uncorrelated Bloch orbitals or whether a localized VB (valence bond) function leads to an improved description in the framework of a SCF one-determinantal approximation. This topic (delocalized vs. localized hole-states derived in the mean-field scheme) is of course inseparably connected to a second point of interest. One would like to know whether symmetry broken hole-states derived in model calculations are of any physical significance in relation to experimental investigations. This fundamental theoretical problem is the subject of the present study.

In recent CO investigations we have analyzed electronic structures of metallomacrocycles in their paramagnetic states (i.e. closed shell systems in the language of molecular quantum mechanics). For this purpose we have developed a semiempirical INDO (intermediate neglect of differential overlap) CO model [24]. The ZDO Hamiltonian has been designed to reproduce the computational results of ab initio methods in organic compounds and transition metal derivatives of the 3d series. To reduce the influence of the residual interaction an all-valence operator with screened experimental two-electron integrals has been employed [25]. Reliable tight-binding results are therefore accessible on the stage of the mean-field approximation. The semiempirical CO investigations offered sufficient theoretical information to discriminate low-dimensional materials into 1D polymers with conducting 3d spines [26–28] and organic metals with ligand-centered transfer channels [29–35]. The various tight-binding calculations lead furthermore to consistent explanations of a large amount of experimental data.

In the present work we want to extend these CO studies from unoxidized transition metal polymers to partially oxidized systems with injected holes that dispose of (significant) transition metal admixtures. The collection of suitable "real" crystals is obviously limited by two conditions: a) Our investigations will be restricted to those 1D materials where the carriers are at least partially confined to the transition metal regime. The majority of the metallomacrocycles, however, belongs to the class of the organic metals [1–5, 26–28, 29–35]. b) Furthermore we want to investigate oxidation states where one electron has been removed from each second molecular stacking unit S. This occupation scheme requires a doubling of the unit cell of the 1D system (i.e. $(S_2)_\infty$, see below). The size of the building block S thus forms a second boundary

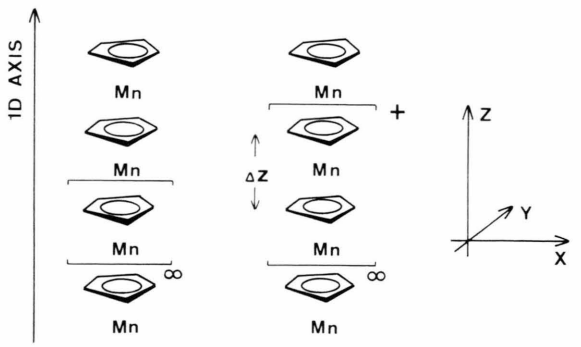

1 MnCp

Fig. 1. Schematic representation of the one-dimensional poly-decker sandwich $(MnCp)_\infty$ **1** composed by cyclopentadienylmanganese(I) fragments as molecular stacking units. The 1D column belongs to the class of the M-L-M materials with 3d centers that are coupled via bridging organic ligands. The employed unit cell dimensions in the crystal orbital investigations of the uncharged solid and the partly oxidized material with one electron removed from each second MnCp moiety embraces two half-sandwiches; this is schematized in the middle of the figure ($[(MnCp)_2]_\infty$ and $[(MnCp)_2^+]_\infty$). The nuclear deformations Δz studied in the numerical calculations are also defined in this representation. The coordinate system is shown on the extreme right; the stacking (1D) axis coincides with the z direction.

depending on the currently available computational facilities. The adopted filling scheme is closely related to the populations encountered in low-dimensional solids that are susceptible to the $4k_F$ (Peierls) lattice distortions [36–38].

It is one purpose of this article to understand possible violations of translation symmetries in partially oxidized 1D solids of the M-L-M group where 3d states are concerned in the transfer channels. In a previous contribution we have analyzed the electronic structure of the partly oxidized tetracyanonickelate(II), $Ni(CN)_4^{2-}$, system which belongs to the M-M solids with direct metal-metal contacts [39]. We have selected the poly-decker sandwich **1** as a representative example in the M-L-M group. The 1D polymer contains the cyclopentadienylmanganese(I), MnCp, moiety as smallest repeat-unit (Figure 1). The infinite $(MnCp)_\infty$ system is yet not characterized. On the other side, various molecular precursors with 12 valence electrons per ML fragment and an alternating arrangement of 3d centers and fivemembered cyclic π ligands have been studied extensively in the past [40, 41]. The electronic structures of conical ML fragments (i.e. molecular stacking units) and triple-decker systems have been analyzed by one-electron procedures of the extended Hückel (EH) type [42, 43]. Semiempirical SCF calculations and theoretical studies beyond the mean-field approximation have been reported for several poly-decker models [41, 44]. The latter contributions as well as a recent tight-binding investigation of various unoxidized $(ML)_\infty$ stacks [28] were based on the INDO operator described in [25].

The plot of the present article is as follows: The essential physical background of the CO investigations on partly oxidized **1** as well as similarities and deliminations to previous solid state and finite molecular approaches are rationalized in the next section. On one side, we make an effort to link the present approach to classical solid state contributions dealing with the importance of localized vs. collective phenomena in extended solids. On the other, the analysis will be related to the conclusions of numerical studies on the nature of hole-states in discrete metal complexes. The crystal orbital calculations on the oxidized MnCp backbone require computational methods beyond the conveniently adopted pure state representation. Suitable model operators for this purpose are statistical ensemble (CO) Hamiltonians which allow for the formation of averaged values over certain manifolds of one-electron states. We make use of the grand canonical (GC) ensemble [45–47]. The implementation of this statistical approximation into the crystal orbital formalism is described in Section 3. Computational conditions are shortly mentioned in the following paragraph. The band structures of the unoxidized and partially oxidized Mn(I) poly-decker chains are studied in 5. Symmetric nuclear coordinates as well as deformations on the optical branch of the lattice modes are considered within the employed unit cell $[(MnCp)_2]_\infty$. A preliminary letter on the electronic structures of partly oxidized **1** and tetracyanonickelate(II) had been published recently [48].

2. Physical Background; Violations of Spatial Symmetries in Finite and Infinite Fermion Systems

Symmetry properties (e.g., spatial, spin, time-reversal) of Fermion systems can be expressed by symmetry operators O_i that commute with the full Hamiltonian H of the N electron system.

$$[H, O_i] = 0 . \tag{1}$$

This commutator equation leads immediately to the relations (2) and (3), respectively, i.e., the exact eigenfunctions Φ_i of H are also eigenfunctions of the symmetry operators O_i.

$$H\Phi_i = E_i\Phi_i , \tag{2}$$

$$O_j\Phi_i = \Delta_i\Phi_i . \tag{3}$$

Recent theoretical investigations on weakly coupled transition metal complexes in their high-lying hole-states, on the other hand, have shown that these conditions are often not fulfilled in variational procedures based on the mean-field (HF) approximation. The solutions of lowest energies are not necessarily symmetry adapted with respect to (some) constants of motion defined by the O_i set. Theoretical tools to investigate these problems are either the Thouless instability conditions [49–51] or Löwdin's symmetry dilemma [52, 53]. Left-right correlations between the transition metal centers often lead to hole-state wave functions with spatially broken solutions [54–61]. The symmetry adapted HF wave functions are unstable, the electronic energy in the mean-field approximation is significantly lowered if the electron has been removed specifically from a single transition metal center. The spatial instability of such a HF wave function simulates a transition in the $(N-1)$ electron system from the inadequate MO (molecular orbital) limit to one of the possible VB (valence bond) structures of the Heitler-London type. The shapes of bands in outer valence photoelectron spectra of some polynuclear 3d complexes have been rationalized in terms of physically feasible localization effects of the 3d electrons upon ionization [62]. The aforementioned left-right correlations between transition metal centers in ionic complexes belong to a class of symmetry violations that are called doublet instabilities [63]. The importance, strength and occurance of various other types of HF instabilities in transition metal systems and their physical consequences have been discussed by several authors [44, 64–66].

The theoretical significance of calculated instabilities in the mean-field approximation (i.e. hole-localization) is determined by the predictive capability of such a computational approach. It is an essential question whether the occurance of a symmetry nonadapted solution is of any experimental reliability or whether (spatially) violated solutions are only a strong reference to the inadequacy of the HF picture. Herring discussed this problem in connection to the stability of spin density waves in a real "correlated" electron gas (in contrast to the ideal Fermi gas) [67]. Calais [68], on the other side, has analyzed this topic with reference to Peierls transitions [69] in extended systems. The essential question is always reduced to the one whether violations of constants of motion (O_i) are still found in theoretical models beyond the mean-field approximation or whether electron correlations prevent the instabilities to occur. Symmetry broken solutions in the latter case are "artifactual" (i.e. model-dependent) and not related to any observable physical quantities.

A general answer to this problem is unfortunately not possible. It is in any case highly desirable to clarify the "significance" of symmetry breaking for every given problem. In charged diatomic and polynuclear clusters this question can be traced back to the evaluation of "repolarization energies" that simulate spatial hole-localizations by CI expansions defined in terms of symmetry adapted (one-electron) basis functions [70, 71]. A symmetry nonadapted solution in the HF approximation is an adequate description of a given open shell state if, and only if, the energy gain due to the observed HF instability is comparable or larger than the energy lowering via repolarization effects and vice versa. This question has been analyzed in some diatomic clusters with 3d or 4d centers [61]. The boundary separating "physical" and "artifactual" solutions in 4d complexes lies at ca. 4 Å and is reduced below 3 Å in 3d derivatives.

The "physical" relevance of symmetry nonadapted solutions can be illustrated in a plain way with reference to time-dependent processes. The localization of holes or the migration of charge carriers are non-stationary processes which cannot be described in terms of canonical (diagonal) time-independent SCF HF (CO) calculations [72]. In the limit of symmetry nonadapted wave functions of "physical reliability" it is often possible to study the time-dependence of the electronic ensemble by means of symmetry broken wave functions of the VB-type. Simply speaking, the process of symmetry breaking simulates the preparation of an initial (quantum) state whose evolution is given by a time-dependent wave function $\Phi(t)$. This is demonstrated in (4) for a simple model with two "VB states" Φ_{I} and Φ_{II}, respectively. We have

$$\Phi(t) = \Phi_{\mathrm{I}}\cos(S_{\mathrm{I/II}}\,t/\hbar) + \Phi_{\mathrm{II}}\sin(S_{\mathrm{I/II}}\,t/\hbar) \tag{4}$$

which, e.g., describes the time evolution of an injected carrier (electron or hole) localized in Φ_I at $t = 0$. $S_{I/II}$ is the overlap amplitude between the two VB-type wave functions. The probability to find the initial carrier at $t \neq 0$ in Φ_{II} reads

$$P(\Phi_{II}) = \sin^2(S_{I/II}\, t/\hbar)\,. \tag{5}$$

The time-scale for the evolution (and thus the time-window accessible to an experimental measurement) can be either a microscopic (see (6)) or a macroscopic one (see (7)); reference is the Bohr's orbit of an electron.

$$(S_{I/II}\, t/\hbar) \geqq 2\pi\,, \tag{6}$$

$$(S_{I/II}\, t/\hbar) \gg 1\,. \tag{7}$$

This short insertion has been given in order to clarify (in the author's view) a possible relation between spatially violated wave functions emerging from a time-independent variational approach and the time evolution of an initially prepared (quantum) state defined in terms of symmetry nonadapted VB wave functions. This argumentation, however, is only a simple, descriptive model far from exact theories of time-dependent phenomena (see [47]). Nevertheless, we feel that this analysis offers some insight into the relevance of HF instabilities in finite or infinite Fermion systems, on one side, and observable time-dependent properties (e.g., hole-localization, migration of charge carriers, etc.), on the other.

The HF instability-investigations on finite Fermion systems (Refs. [54–66]) have been mentioned in some detail on account of their close relation to classical solid state contributions on the validity of collective and localized effects in transition metal systems with half-filled shells. Mott [73], Goodenough [74] as well as Robin and Day [75–77] discussed the importance of itinerant and local electrons either by intuitive physical arguments or by highly idealized model operators of the Hubbard-type. The remarkable similarities between electronic structure effects in finite (Refs. [54–66]) and infinite (Refs. [73–77]) Fermion systems has been clarified by Whangbo in several thorough contributions [78, 79].

The physical basis of the present investigation shows furthermore formal analogies to recent theoretical contributions that have been published in connection with the well-known Mott insulators (e.g., simple transition metal oxides) [80]. In this context we have to mention Alder and Feinleib who made the ad hoc assumption that some electrons in transition metal oxides (e.g., NiO, CoO, FeO) exist in band states while 3d states are assumed to be atomically localized [81]. The solid state models of Brandow are based local moment HF theories leading to variational wave functions of lower spatial symmetries [82, 83]. Brandow derived also simplified relations to recognize the onset of localization and to define domain boundaries between metals, insulators and antiferromagnetic insulators. The most detailed contributions on Mott insulators have been published by Kunz and coworkers [84–86]. These authors have reinvestigated an original suggestion of Seitz [87] representing hole-states in periodic systems by spatially uncorrelated Bloch orbitals. This assumption had been formulated on the basis of the one-to-one correspondence of Bloch (i.e. delocalized MO functions in finite systems) and Wannier (i.e. VB orbitals of the Heitler-London type) states in solids with completely filled shells. This coalescence, however, is more and more perturbed in partly oxidized systems with narrow HF dispersions. Kunz et al. have shown that the best single determinant description in the case of "broad" holes is given by Bloch orbitals that lead to a reduction of the kinetic energy. "Narrow" holes, on the other side, find their adequate description in terms of localized VB wave functions which allow for an energy lowering due to local reorganization processes. The predominance of band or localized electronic effects in partly oxidized 1D materials is controlled by the ratio of the kinetic energy of the electrons and the possible gain in energy due to incoherent (local) reorganization processes in the corresponding hole-states. This review of recent solid state investigations demonstrates immediately the challenging theoretical problem to analyze the spatial hole-state properties in complex metallo-macrocycles.

The large unit cell dimension of **1** causes additional necessary restrictions in the variational degrees of freedom [79]. Magnetic effects between the spins of the electrons are neglected which would lead to 2^N possible spin configurations of the Ising-type. The inherent problems associated with spin interactions have been analyzed previously in the framework of a single-band Hubbard-Hamiltonian [88]; an extension to complex solids seems to be

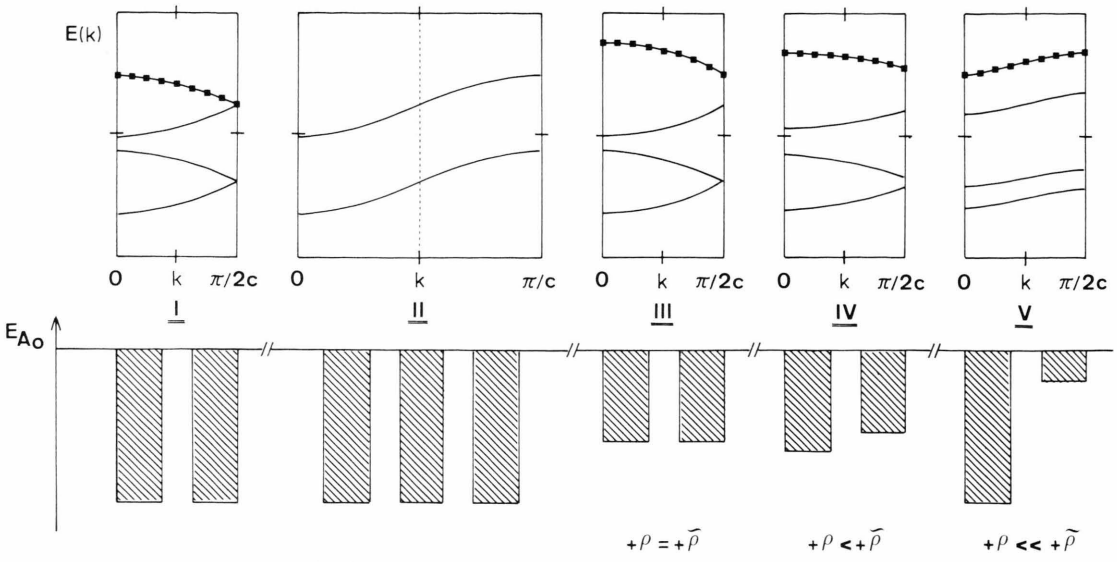

Fig. 2. Simplified displays **I** – **V** of dispersion curves $\varepsilon(k)$ (top, k-space representation) and one-center energies E_{A_0} (A = S) (bottom, real-space representation) of the one-dimensional solid S_∞ containing two stacking fragments S per unit cell ($[(S)_2]_\infty$, **I** and **III** – **V**). The first Brillouin zone of the 1D materials **I**, **III** – **V** is defined within the interval $0 \leqq k \leqq \pi/2c$; the zone scheme of **II** corresponds to $0 \leqq k \leqq \pi/c$, i.e. the repeat-unit associated with the second diagram is a single S fragment. c stands for the interplanar spacing between adjacent S layers. The $\varepsilon(k)$ diagrams are k-space representations of possible symmetry reductions in partly oxidized 1D systems; the E_{A_0} figures are simplified real-space representations to identify the translation symmetry encountered in the 1D materials. The "half-filled" bands are symbolized by black squares. The two diagrams (i.e. $\varepsilon(k)$ and E_{A_0}) on the extreme left of the figure, **I**, correspond to dispersion curves and mono-center energies of a solid with completely filled dispersions (unoxidized chain). The $\varepsilon(k)$ plot shows the characteristic Herring's degeneracies at the (assumed) X-point indicating that the full band structure information is already contained in the second representation **II** with a bisected unit cell and a doubled Brillouin zone. The energy dispersions of **I** and **II** are simply related by folding back the latter $\varepsilon(k)$ curves at the middle (dotted line) of the zone scheme. The band pattern on the lhs. of the figure is derived in the framework of the SCF HF CO formalism only for unoxidized 1D materials with completely filled HF dispersions. On the other hand, it has to be mentioned that this scheme is always found in CO approaches based on one-electron crystal Hamiltonians which are independent from the number of electrons. Identical $\varepsilon(k)$ relations are thus derived for unoxidized and partly oxidized crystalline solids by means of these simple procedures. The third couple, **III**, of the $\varepsilon(k)$ and E_{A_0} plots describes a symmetry adapted SCF solution of a oxidized column ($+\varrho = +\tilde{\varrho}$). One electron has been removed from each second S unit ($+\varrho = 0.5$). The averaged oxidation state leads immediately to a common one-center potential E_{A_0}. The translation symmetry of the oxidized strand corresponds to the symmetry properties of the unoxidized backbone. The remaining displays **IV** and **V** symbolize theoretical results with spatially violated wave functions. **IV** and **V** are associated to CO solutions with different charge distributions $+\varrho \neq +\tilde{\varrho}$ and one-center energies $E_{A_0} \neq \tilde{E}_{A_0}$ at the two sites S within the employed stacking-units. The violations of the spatial symmetry in **V** exceed the perturbations schematized in **IV**. In the latter $\varepsilon(k)$ diagram it is still possible to relate the energy curves of the oxidized polymer to upper and lower branches of the Hartree-Fock dispersions of the unoxidized crystal. This one-to-one correspondence is strongly perturbed in the last display with HF energy bands that are either prevailingly related to the $+\varrho$ or the $+\tilde{\varrho}$ domain, respectively.

impossible. Spin-quantum numbers are therefore undefined in the statistical CO approach. It is assumed that the CO wave functions derived via the GC crystal Hamiltonian correspond to averaged "spin-states" containing all Ising-type configurations from the ferromagnetic coupling scheme, on one side, to the antiferromagnetic limit, on the other. The CO approach is furthermore restricted to partly oxidized states that are insulating, i.e. all microstates in a given "half-filled" band are singly occupied. It is well-known that this filling scheme corresponds to the ground state population of narrow-band materials [7, 79] that are models for the idealized Wigner crystal in the low-density limit [89]. Some surprising analogies between organometallic polymers and the physical properties of the idealized Wigner lattice have been discussed in one of our previous papers [26].

The employed restrictions of the present approach lead to a close interrelation between the subsequent CO investigations within the GC averaging-procedure and the problem of doublet instabilities

in cationic hole-states of finite complexes. Furthermore all those difficulties are avoided that are found in comparative CO investigations on non-paramagnetic and paramagnetic materials [90, 91]. The described limitations in the variational degrees of freedom, however, are the sources of some differences between the present analysis and previous theoretical studies where the doubling of the unit cell is accompanied by a metal-to-insulator transition. Slater [92], Matsubara and Yokota [93] as well as des Cloizeaux [94] investigated this phase transition via the introduction of an antiferromagnetic sublattice, while Peierls [69], Goodenough [95] as well as Alder and Brooks [96] discussed the problem in terms of displacements of the nuclear coordinates. The similarities between the above mentioned Mott-type correlations and Peierls instabilities have been analyzed in a very recent article [97].

The basic principles on the physical background of the present work are schematized in Figure 2. We have collected dispersion curves $\varepsilon(k)$ (top) and one-center potentials, E_{A_0} (bottom, see next section), of a one-dimensional polymer S_∞; the drawings are associated with several filling schemes of the HF bands and different translation symmetries encountered in the 1D backbone (i.e. possible formation of superstructures). The employed stacking-unit contains two S fragments and the first Brillouin zone is defined within the interval $0 \leqq k \leqq \pi/2c$; k is of course the wave vector characterizing the translational symmetry in the 1D material and c stands for the separation between adjacent S moieties. The HF bands of the uncharged $(S_2)_\infty$ model (completely filled levels) are displayed on the extreme left of Figure 2 (**I**). The dispersion curves show the characteristic Herring's degeneracies [98] at the edge of the Brillouin zone (X-point) indicating that the smallest possible repeat-unit of the 1D system with the full translational symmetry is given by a single S fragment. The band structure of the neutral backbone is completely described by the $\varepsilon(k)$ diagram **II** which is associated with a zone scheme $0 \leqq k \leqq \pi/c$. The HF bands of **I** are related to the latter plot by folding back the dispersions of **II** at the middle of the first Brillouin zone ($k = \pi/2c$). Such a one-to-one mapping between the $\varepsilon(k)$ curves of **I** and **II**, however, is only found in 1D stacks with primitive translation symmetries. Combined symmetry operations (e.g., screw or helical axes, glide planes) lead to additional symmetry relations between the two sets of $\varepsilon(k)$ curves. Detailed informations on this topic can be found in text books of symmetry principles of solids [99]. Tight-binding models based on simplified one-electron Hamiltonians (e.g., Wolfsberg-Helmholtz (WH), extended Hückel (EH) or Su-Schrieffer-Heeger (SSH) procedures) give always raise to dispersion patterns as shown on the lhs. of Figure 2. The positions and the shapes of the bands are independent from the number of electrons (i.e. from the elements of the charge-density-bond-order matrices). Important solid state properties of materials with injected carriers are hence beyond the scope of the latter CO techniques.

The remaining diagrams in Figure 2 symbolize band structures and one-center potentials of partly oxidized models characterized by a single "half-filled" HF dispersion in the GC formalism. The atomic potentials E_{A_0} and the degree of oxidation $+\varrho$ in diagram **III** are identical in both S fragments per unit cell (i.e. $[(S^{+\varrho}S^{+\varrho})_2]_\infty$). The full translational symmetry is conserved. These conditions are to be expected in 1D materials with "broad" energy bands $\varepsilon(k)$ and/or small on-site Coulomb repulsions U, i.e. for solids that are far from the "low-density limit" of the Wigner crystal. Violations of translation symmetries are represented in the diagrams **IV** and **V**, respectively. The two plots symbolize 1D systems with an alternating arrangement of different oxidation states $+\varrho$ and $+\tilde{\varrho}$ as well as one-center energies E_{A_0} and $\tilde{E}_{A_0}$. The mutual charge separation $\Delta\varrho = (+\varrho) - (+\tilde{\varrho})$ and the difference in the one-center energies $\Delta E_{A_0} = E_{A_0} - \tilde{E}_{A_0}$ are small in **IV** but are remarkably enlarged in the last display **V**. It is a straightforward procedure to relate the HF bands of **IV** (with the reduced translation symmetry) to their $\varepsilon(k)$ parents associated with the unoxidized chain or the symmetry adapted polymer, respectively. This simple correlation to the upper and lower branches encountered in **I** and **III** is impossible in the case of **V** where electronic reorganization effects are so strong that the HF dispersions of the two oxidation states $+\varrho$ and $+\tilde{\varrho}$ are no longer coupled in k-space (i.e. upper and lower branches of an $\varepsilon(k)$ pair with X-degeneracies in **I** (and **III**)). Energy bands and E_{A_0} figures as shown in **IV** and **V** must be expected for solids that are close enough to the low-density limit of the Wigner crystal. The alternating arrangement of the one-center energies $\ldots E_{A_0}, \tilde{E}_{A_0}, E_{A_0}, \tilde{E}_{A_0}, \ldots$ with $E_{A_0} \neq \tilde{E}_{A_0}$ illustrates some formal analogies between the electronic struc-

tures of mixed valence systems and semiconductor superlattices [100]. The building blocks in the former materials are of identical stoichiometry and topology but condensate into an arrangement with inequivalent electronic populations. Different atomic species, on the other hand, are found in the two domains of (semiconductor) superlattices.

The HF energy bands displayed in **IV** and **V** are nevertheless derived for 1D materials that are subject to periodic boundary conditions. The symmetry properties of the Bloch functions in the "mixed valence systems", however, are modified with respect to the irreducible representations spanned by the wave vector k. The conservation of certain translation symmetries is of course a direct consequence of the employed occupation scheme (i.e. removal of one electron per two S fragments). These conditions permit one to study spatial violations of crystal orbitals that are still feasible in terms of "Bloch orbitals" and elude the application of extended symmetry projections on trial VB functions that have been suggested by Kunz [86].

3. The Grand Canonical (GC) Averaging-Procedure in the Crystal Orbital Formalism

In statistical mechanics the grand canonical (GC) ensemble is adopted to describe thermodynamic equilibria. This classical definition is not used in the present crystal orbital study. We will employ the GC ensemble as a rather formal scheme which allows for the formation of averaged values over certain manifolds of one-particle states. The electrons in the "partly filled regimes" are smeared out statistically. The GC averaging-technique can be applied in one- and many-electron approaches to the ground state and excited states [45, 46]. The ensemble formalism based on (fractal) occupation numbers n_i is combined with the convienent SCF HF CO ansatz. The method belongs to a hierarchy of models in electronic structure theory where states under consideration are always described in terms of statistical or fractional occupations. Widely-used procedures in this class are the atomic hyper-Hartree-Fock formalism [101], the transition state (TS) model of Slater defined in the X_α approximation [102], the LCAO extension of the TS technique, the transition operator method (TOM) used for ionization and attachment processes in molecules [103, 104] as well as the popular "half-electron" models in semiempirical MO procedures [105]. Statistical Hamiltionians in the tight-binding formalism have been adopted to improve the description of the empty Fermi sea in insulators and semiconductors [106], to study the solid state properties of segregated donor and acceptor chains [107] and to analyze solitons and polarons in polyacetylene [108].

To derive the GC HF operator in the CO scheme field operators $\psi(r)$ and $\psi^+(r)$ are defined in terms of an orthogonal basis $\chi_i(r)$ and annihilation – creation operators c_i and c_i^+, that obey the convenient anticommutation rules of (10).

$$\psi(r) = \sum_i \chi_i(r)\, c_i\,, \tag{8}$$

$$\psi^+(r) = \sum_i \chi_i(r)\, c_i^+\,, \tag{9}$$

$$\begin{aligned} [c_i, c_j]_+ &= c_i c_j + c_j c_i = 0\,,\\ [c_i^+, c_j^+]_+ &= c_i^+ c_j^+ + c_j^+ c_i^+ = 0\,,\\ [c_i, c_j^+]_+ &= c_i c_j^+ + c_j^+ c_i = \delta_{ij}\,. \end{aligned} \tag{10}$$

It is convenient to define occupation numbers $n_i = c_i^+ c_i$ in the case of a canonical one-particle basis diagonalizing the HF (CO) operator; the n_i set fulfills the idempotency relation (11).

$$n_i^2 = n_i\,. \tag{11}$$

The statistics of the N electron system defined via the n_i figures is given by the grand canonical partition function Z

$$Z = \mathrm{Tr}\exp\left[-(H_{\mathrm{HF}} - \mu N_i)/\theta\right], \tag{12}$$

where H_{HF} is the mean-field (HF) operator, μ the chemical potential and θ the absolute temperature (in energy units). The number operator N_i reads $N_i = \sum_i n_i$. The GC density operator ϱ_{GC} is defined in (13) by using the partition function Z; the GC averaging for any operator O is displayed in (14).

$$\varrho_{\mathrm{GC}} = Z^{-1}\exp\left[-(H_{\mathrm{HF}} - \mu N_i)/\theta\right], \tag{13}$$

$$\langle O\rangle_{\mathrm{GC}} = \mathrm{Tr}\, O\varrho_{\mathrm{GC}}\,. \tag{14}$$

A canonical (diagonal) one-particle basis allows for the factorization of ϱ_{GC} into the product (15) with parameters λ_i that are given in (16).

$$\varrho_{\mathrm{GC}} = \prod_i \left[(1 + \lambda_i n_i)/(2 + \lambda_i)\right], \tag{15}$$

$$\begin{aligned} \lambda_i &= \exp\left[-(\varepsilon_i - \mu)/\theta\right] - 1\,,\\ \varepsilon_i &= \text{one-particle energy of the } i\text{-th state.} \end{aligned} \tag{16}$$

The averaged population of the i-th (one-particle) state is defined in (17) which leads immediately to an expression for ϱ_{GC} where reference to thermodynamic data (μ, θ) is no longer necessary.

$$\langle n_i\rangle_{GC} = (1+\lambda_i)/(2+\lambda_i) = [1+\exp(\varepsilon_i-\mu)/\theta]^{-1}, \quad (17)$$

$$\varrho_{GC} = \prod_i [1-\langle n_i\rangle_{GC} - (2\langle n_i\rangle_{GC}-1)\, n_i]. \quad (18)$$

The subsequent relations (19)–(21) follow directly from the definition of the ϱ_{GC} operator.

$$\langle n_i n_j\rangle_{GC} = \langle n_i\rangle_{GC}\langle n_j\rangle_{GC}, \quad (21)$$

$$\langle c_i^+ c_j\rangle_{GC} = \langle n_i\rangle_{GC}\delta_{ij}, \quad (20)$$

$$\langle c_i^+ c_j^+ c_k c_l\rangle_{GC} = \langle n_i\rangle_{GC}\langle n_j\rangle_{GC}[\delta_{il}\delta_{jk} - \delta_{ik}\delta_{jl}]. \quad (19)$$

The last expressions make it to a straightforward procedure to define the k-dependent pseudoeigenvalue problems in the SCF HF CO formalism combined with the GC averaging-technique. The basic principles of the CO approach, however, are not reviewed in larger detail in this manuscript (see [13] and [14]). The complex Hermitean pseudoeigenvalue problem in the ZDO basis is defined in (22). $H_{HF}(k)_{GC}$ is the Fock operator in the GC scheme which depends parametrically on the wave vector k. The one-electron energies that form the HF dispersions are abbreviated by $\varepsilon(k)$ and the $c(k)$ figures stand for the variational coefficients of the CO wave functions. The Fourier sum in (23) is a real space representation of the Fock operator. The index j has been used to label the unit cells in the 1D column ($j=0$, reference cell in the origin, $j=\pm1, \pm2, \ldots \pm\infty$, first, second, etc. nearest neighbors).

$$H_{HF}(k)_{GC}\, c(k) = \varepsilon(k)\, c(k), \quad (22)$$

$$H_{HF}(k)_{GC} = \sum_{j=-\infty}^{+\infty} \exp(ijk)\, H_{HF}(j)_{GC}. \quad (23)$$

A decomposition of $H_{HF}(k)_{GC}$ into the core Hamiltonian $H(k)_{GC}$ (i.e. kinetic energy of the electrons and electron-core attraction) and the two-electron part $G(k)_{GC}$ in the mean-field approximation is shown in (24); the explicit formulae for the determination of $H(k)_{GC}$ have been reported in a previous article [24].

$$H_{HF}(k)_{GC} = H(k)_{GC} + G(k)_{GC}. \quad (24)$$

The two-electron part $G(k)_{GC}$ can be expressed in terms of electron-electron (AO) basis integrals and elements of the charge-density-bond-order matrix $P(j''-j')_{\lambda\sigma,GC}$ which depend on the statistical occupation numbers $\langle n_i\rangle_{GC}$. Equation (25) has been derived without any approximations and is valid for full overlap ab initio CO calculations. The remarkable simplifications in ZDO-based CO models are discussed in [24].

$$G_{\mu_0\nu_j,GC} = \sum_{j',j''=-\infty}^{+\infty} P(j''-j')_{\lambda\sigma,GC} \cdot [(\mu_0\nu_j\,|\,\lambda_{j'}\sigma_{j''}) - (1/2)\,(\mu_0\sigma_{j''}\,|\,\lambda_{j'}\nu_j)]. \quad (25)$$

The charge-density-bond-order matrix $P(j''-j')_{\lambda\sigma,GC}$ has to be determined by numerical integration within the first Brillouin zone as a function of the $\langle n_i\rangle_{GC}$ parameters and leads thus to a coupling of the k-dependent pseudoeigenvalue problems of (22).

$$P(j''-j')_{\lambda\sigma,GC} = (\tilde{c}/2\pi\langle N_i\rangle_{GC}) \int_{-\pi/\tilde{c}}^{+\pi/\tilde{c}} \sum_i \langle n_i\rangle_{GC} \cdot c^*(k)_{i\lambda}\, c(k)_{i\sigma} \exp[ik(j''-j')]\, dk; \quad (26)$$

$\tilde{c}$ = unit cell dimension (= $2c$ in the poly-decker sandwich compounds). – Equations (25) and (26), respectively, display immediately the simple structure of the CO formalism based on the GC averaging-procedure. The summation over the filled, half-filled and empty Fermi seas [26] is controlled by the statistical $\langle n_i\rangle_{GC}$ spectrum. In the present contribution $\langle n_i\rangle_{GC}$ is restricted to the trivial integers 2, 1 and 0 for the above mentioned subspaces of the Fermi sea. $\langle n_i\rangle_{GC}=1$ is adopted for the half-filled band in partly oxidized MnCp backbones where all k-dependent microstates are singly occupied. The two integers $\langle n_i\rangle_{GC}=2$ and 0 ($\langle n_i\rangle_{GC}\neq1$) reduce the statistical eigenvalue problems (22) to the convenient standard form of the SCF HF CO formalism. The validity of the GC averaging-procedure, however, is not restricted to nonfractional $\langle n_i\rangle_{GC}$ numbers; the statistical approach can be extended to any ensemble of occupation numbers $\langle n_i\rangle_{GC}\neq\in$ (integer) and <2 defining certain electronic manifolds (see [107]).

The total energy of the 1D polymer in the GC formalism is given in (27); E_{TOT} has been normalized to one unit cell and E_C stands for the repulsion between the atomic cores.

$$E_{TOT} = \sum_{j=-\infty}^{+\infty} \sum_{\mu,\nu} (1/2)\, P(j)_{\mu\nu,GC} \cdot [H(j)_{\mu\nu,GC} + H_{HF}(j)_{\mu\nu,GC}] + E_C. \quad (27)$$

In order to simplify the analysis of the computational results in Section 5 we make use of a partitioning scheme for E_{TOT} which allows for the fragmentation of the total energy into one- and two-center elements in computational approaches based on the ZDO approximation [24, 109].

$$E_{TOT} = \sum_{A_0} E_{A_0} + \sum_{A_0 < B_0} E_{A_0 B_0} + \sum_{j} \sum_{A_0} \sum_{B_j} E_{A_0 B_j} . \qquad (28)$$

The first expression on the rhs. of (28) stands for the one-center energies of the atoms A (defined in (29)) while the remaining sums correspond to diatomic interaction energies of the intra- and intercell types.

$$E_{A_0} = E_{A_0}^{U} + E_{A_0}^{COU} + E_{A_0}^{EX} , \qquad (29)$$

$$E_{A_0 B_j} = E_{A_0 B_j}^{RES} + E_{A_0 B_j}^{COU} + E_{A_0 B_j}^{EX} ,$$

$$j = 0 \rightarrow E_{A_0 B_0} , \quad j \neq 0 \rightarrow E_{A_0 B_j} . \qquad (30)$$

The expressions on the rhs. of (29) and (30) contain well-defined quantities. $E_{A_0}^{U}$ is the atomic core potential at the A-th center, $E_{A_0}^{COU}$ represents the on-site electron-electron repulsion (i.e. the classical Coulomb potential) and $E_{A_0}^{EX}$ is the abbreviation for the exchange energy (i.e. Fermi correlation) that must be traced back to the antisymmetry of the HF determinant. Similar expressions are valid for the two-center couples $E_{A_0 B_0}$ and $E_{A_0 B_j}$, respectively. $E_{A_0 B_j}^{RES}$ symbolizes the "resonance" interaction between the atomic sites A and B (i.e. kinetic "hopping" energy of the electrons). The electrostatic interaction is given by the sum of electron-electron and core-core repulsions and the electron-core attraction. The analytic expressions for these interaction parameters are derived in [24] for "closed shell" polymers. All coupling terms are given by products of interaction integrals (e.g., electron-electron, electron-core, kinetic energy) in the AO basis and elements of the bond-order matrices. The $P(j'' - j')_{\lambda\sigma}$ figures of [24] have to be replaced by the corresponding $P(j'' - j')_{\lambda\sigma,GC}$ elements of (26) to extend the energy fragmentation to the GC ensemble.

4. Computational Details

The numerical quality of CO calculations is both influenced by the number of employed k-points considered in the pseudoeigenvalue problems and by the dimension of the lattice sum expansion [110, 111]. The k-dependence is usually weak in comparison to the convergence properties of the lattice sum. On the basis of our previous computational experience we have solved (22) at 10 points in k-space and determined the lattice sums in the fifth neighbor's approximation.

The iterative SCF steps have been controlled via an accelerated Hartree damping of the charge-density-bond-order matrices to prevent filling-up instabilities between the occupied, half-filled and empty Fermi seas during the SCF cycles [112]. Trial wave functions of the WH-type have been used to start the tight-binding calculations on the unoxidized Mn(I) material. The SCF CO wave functions of the uncharged parent **1** have been employed as input for the subsequent calculations on the oxidized system. Tight-binding studies with different (band) occupation schemes have been performed in order to guarantee to locate the "true" variational minimum within the allowed degrees of freedom. We have tried to detect both spatially nonviolated and spatially violated SCF solutions in the 1D material with injected holes. Oxidation processes within all occupied "Mn 3d" valence bands (i.e. $3d_{z^2} = 3d\sigma$, $3d_{x^2-y^2}/3d_{xy} = 3d\delta$) have been taken into account. The lowest energy in the oxidized chains is predicted for holes disposing of significant Mn $3d_{z^2}$ admixtures (see next section). A severe SCF energy criterion of 10^{-5} au has been adopted to terminate the iterative steps. The tight-binding calculations on **1** have been performed on IBM 370/168 and CRAY-1 computers and require ca. 4–6 h CPU time on the first machine and ca. 30–45 min on the latter one.

The HF bands of the charged MnCp chain would be predicted at unrealistic energies if the electrostatic interactions with the counterions in the real lattice (i.e. acceptor stacks involved in the charge transfer events) is neglected. Different models have been developed in the past years to simulate these environment effects in ZDO-based calculations on finite clusters [113] or low-dimensional materials [107, 114, 115]. The electrostatic potentials $V_{\mu\nu}^{el}\,\delta_{\mu\nu}$ created by the "external layers" enter only the diagonal-elements of the Fock operator in MO or CO procedures. To reduce the computational expenditure of the present approach we have renounced to calculate these $V_{\mu\nu}^{el}\,\delta_{\mu\nu}$ elements explicitly but made the rough assumption that all correction terms can be approximated by a single shift parameter that has been chosen to match the centers of

gravity of the HF dispersions of the unoxidized and partly oxidized Mn(I) chains. The validity of this approach has been tested in thorough model calculations on simple solids [116]. The employed approximation is furthermore consistent with the suggestion that a decreasing number of electrons **1** is related to an increasing number of acceptor moieties in the real crystal.

The density of states distributions, $N(E)$, have been determined by a discrete sampling procedure over $N_k = 50000$ k-points per $\varepsilon(k)$ curve [117]. To evaluate these N_k figures we expanded the energy bands of **1** into fourth order polynomials calculated by a least squares approximation to the 10 available k-points. Characteristic geometrical parameters of poly-decker sandwich compounds have been used in the CO calculations [41, 118]. The employed MnC separation in the unoxidized stack is 2.06 Å while CC bond lengths of 1.44 Å have been selected. A standard value of 1.1 Å has been used for the CH bonds [119]. The unit cell dimension of a single MnCp stacking unit is 3.30 Å (= 6.60 Å for the doubled cell employed in the subsequent calculations). The considered geometrical deformations are schematized in Figure 1. The band structures of the unoxidized and the charged materials have been investigated for displacement coordinates Δz between 0 and 0.2 Å. This interval is typically found in metallocene pairs with $3d^6/3d^5$ occupations [120].

5. Results and Discussion

The $\varepsilon(k)$ curves and the density of states distributions, $N(E)$, of the highest filled HF bands of the uncharged polymer **1** are displayed in Fig. 3; the selected 14 eV window spans an interval from -20 eV to -6 eV. Three characteristic displacement coordinates Δz have been chosen for this representation, the symmetric 1D arrangement with $\Delta z = 0$ Å and two distorted modifications with $\Delta z = 0.1$ Å and $\Delta z = 0.2$ Å, respectively. The energy grid in the $N(E)$ histograms amounts to 0.15 eV. All $N(E)$ diagrams have been normalized by a common scale factor (i.e. the representations in the Figs. 3 and 4).

The characteristic Herring's degeneracies at the X-point are easy to identify in the $\varepsilon(k)$ plot on the top of Fig. 3 ($\Delta z = 0$ Å). The perturbations of the degeneracies for $\Delta z \neq 0$ are largest in the lowest HF dispersions shown in Figure 3. Smaller marginal

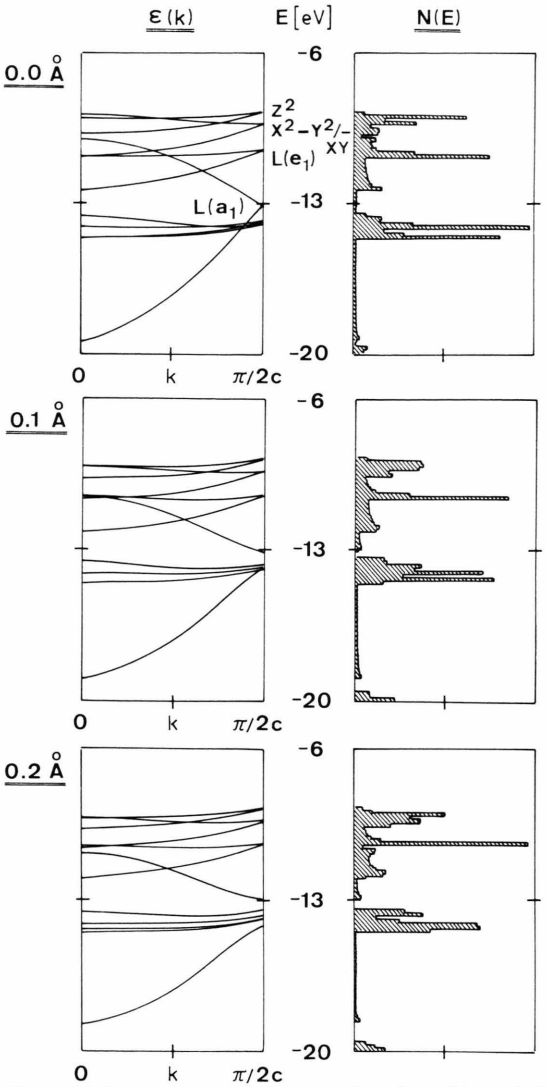

Fig. 3. Highest occupied HF energy bands, $\varepsilon(k)$, and density of states distributions, $N(E)$, of the unoxidized Mn(I) poly-decker column **1** for displacement coordinates (see Fig. 1) $\Delta z = 0$ Å (top), $\Delta z = 0.1$ Å (middle) and $\Delta z = 0.2$ Å (bottom), respectively. The employed unit cell embraces two MnCp fragments. The $\varepsilon(k)$ relations and the $N(E)$ histograms are displayed in a 14 eV window in the interval between -20 eV to -6 eV. The Herring's degeneracies at the (assumed) edge of the Brillouin zone are easy to identify in the upper plot. The characters of the CO wave functions are labeled in the $\varepsilon(k)$ representation of the spatially unperturbed 1D material. The following abbreviations have been used: z^2: Mn $3d_{z^2}$ dispersion; x^2-y^2/xy: Mn $3d_{x^2-y^2}/3d_{xy}$; L: cyclopentadienyl ligand; L (e_1): degenerate e_1 ligand π band; L (a_1): totally symmetric a_1 ligand π band. The density of states distributions have been calculated by means of a discrete sampling technique; the energy grid employed for the construction of the $N(E)$ histograms amounts to 0.15 eV. A common normalization factor has been used to scale the three $N(E)$ representations in the figure (and to normalize the $N(E)$ maxima in Figure 4).

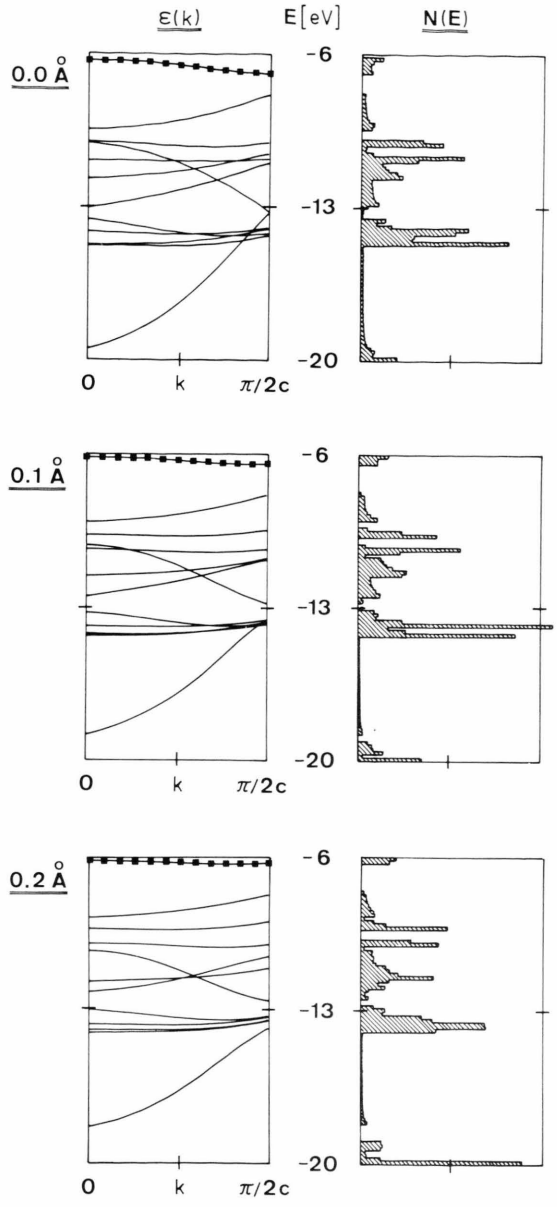

gaps $\Delta\varepsilon(k = \pi/2c)$ in the perturbed structures are predicted for the highest filled bands. The characters of the CO wave functions are labeled in the $\varepsilon(k)$ plot on the top of the figure. The valence band of the unoxidized chain (X-point) is of Mn $3d_{z^2}$ character. The CO microstates contain also small destabilizing admixtures from the totally symmetric ligand π (a_1) states. The subsequent dispersion curves are associated with degenerate Mn $3d_{x^2-y^2}$/ various $\varepsilon(k)$ curves. The $\Delta\varepsilon$ parameter of the $3d_{xy}$ states of e_2 symmetry (the irreducible representations correspond to C_{5v} symmetry) which are mixed with ligand σ orbitals at the Γ-point. The Cp admixtures at the zone edge, on the other hand, are π-type functions. The relative sequence between the "Mn 3d bands" of a_1 and e_2 symmetry is changed at the zone center; the highest occupied microstates at the Γ-point belong to the e_2 subspace. The 3d amplitudes in the CO wave functions of the three (six) highest filled bands exceed in any case 70%. The localization properties of the CO's are nearly k-independent. The subsequent outer valence bands of unoxidized **1** are associated with ligand π states of e_1 and a_1 symmetry. The remaining $\varepsilon(k)$ curves which are predicted in the center of gravity of the lower a_1 dispersion are high-lying σ-ribbon linear combinations. The corresponding HF bands are quite flat as a result of the small metal-ligand overlap. The band sequence in **1** is comparable with the results of INDO MO calculations on discrete complexes containing the MnCp half-sandwich [121, 122]. The band widths, $\Delta\varepsilon$, of the $\varepsilon(k)$ curves in Fig. 3 are found in an interval between 0.6 eV for the "Mn $3d_{z^2}$" dispersion and 9.2 eV predicted for the ligand π band of a_1 symmetry. These numbers refer always to the upper and lower branches of the

Fig. 4. Highest occupied HF energy bands, $\varepsilon(k)$, and density of states distributions, $N(E)$, of the partly oxidized poly-decker sandwich $[(MnCp)_2^+]_\infty$ for displacement coordinates (see Fig. 1) $\Delta z = 0$ Å (top), $\Delta z = 0.1$ Å (middle) and $\Delta z = 0.2$ Å (bottom), respectively. The employed stacking unit corresponds to two MnCp fragments. The $\varepsilon(k)$ relations and the $N(E)$ histograms are displayed in a 14 eV window which is comparable with the energetic interval selected in the uncharged 1D columns (Figure 3). The absolute values of the HF dispersions of the oxidized materials have been shifted in order to match the $\varepsilon(k)$ spectrum of the uncharged polymer. The perturbations of the Herring's degeneracies at the X-point due to the reduction of the translation symmetry can be seen in the $\varepsilon(k)$ plot on the top of the figure. Significant violations of the $\varepsilon(k)$ curves in the $\Delta z = 0$ Å arrangement are restricted to the "Mn 3d" dispersions. The superposition of electronic factors (i.e. reorganization processes of the electrons in the hole-states) and nuclear deformations (i.e. Δz numbers $\neq 0$) on the structures of the $\varepsilon(k)$ curves is made plain due to the comparison of the Figs. 3 and 4. The "half-filled" dispersion curves of the partly oxidized 1D material **1** are labeled by black squares. The energy grid used for the construction of the $N(E)$ maxima is identical with the $\Delta\varepsilon$ interval employed in Fig. 3 (0.15 eV). The $\varepsilon(k)$ and $N(E)$ diagrams of the $\Delta z = 0$ Å material are associated with the symmetry broken ($q_{Mn} \neq \bar{q}_{Mn}$) ground state of the partly oxidized poly-decker.

"Mn $3d_{x^2-y^2}/3d_{xy}$" bands exceeds slightly the width of the "Mn $3d_{z^2}$" curve (1.1 eV vs. 0.6 eV).

The dispersion curves and the $N(E)$ histograms of the polymer with one electron removed per two MnCp sites are shown in Fig. 4 in a 14 eV window which is comparable to that of Fig. 3. The injected holes are confined to the totally symmetric a_1 regime (i.e. descendant of the highest filled band of the unoxidized chain) and contain admixtures both from the Mn $3d_{z^2}$ orbitals (26%) and, to a larger extend, from the ligand subspace (π and σ states, 74%). The metal-ligand ratio encountered in the hole-states of the oxidized material is a first hint to significant electronic reorganizations accompanying the injection of the carriers. Such orbital rearrangement processes in cationic hole-states are well-known phenomena in transition metal complexes of the 3d series and have been studied in some detail in connection with low-energy photoelectron spectra of 3d derivatives [123, 124].

The comparison of the two upper $\varepsilon(k)$ plots in the Figs. 3 and 4 shows the pronounced violations of the X-degeneracies of the unoxidized chain in the charged material. Prevailingly those HF dispersions are perturbed that contain remarkable Mn 3d admixtures in the CO wave functions while the X-degeneracies of ligand bands are only slightly lifted. The significant separation between the "filled" and "half-filled" a_1 curves is of course expected. Figure 4 shows furthermore that also the two $\varepsilon(k)$ branches differ in their analytic structures. The two lower representations in Figs. 3 and 4 indicate at once roughly comparable perturbations of the HF bands either due to hole-injection or due to the symmetry reduction via nuclear displacements (Δz). The $N(E)$ distributions of the uncharged chain, on one hand, and the oxidized column, on the other, differ significantly. The energetic separation between the outer valence bands is enlarged in the oxidized 1D material where the widths of the HF dispersions is reduced by a factor of ca. 2.

The HF energy bands and the $N(E)$ distributions of the two highest filled bands (precisely: the highest filled and half-filled dispersions) of the oxidized 1D stack are collected in Fig. 5 for four representative Δz coordinates. We have chosen once again the symmetric arrangement with $\Delta z = 0$ Å as well as the displaced stacks with $\Delta z = 0.1$ Å and $\Delta z = 0.2$ Å, respectively. The band structure properties for an infinitesimal displacement coordinate $\Delta z = 0.001$ Å are additionally given in this display. The various $\varepsilon(k)$ diagrams show the remarkable modifications in the electronic structure of the charged polymer for extremely small deformations of the nuclear framework. It must be expected that strong reorganizations of the electrons are operative in the oxidized strand in the vicinity of the totally symmetric unit cell with $\Delta z = 0$. This behaviour reminds one strongly to "sudden polarization effects" discussed in the excited states of molecules [125–127].

Table 1. Calculated net charges q_A in the unoxidized MnCp polymer **1** as well as the oxidized chain with one electron removed from each second half-sandwich moiety according to the semiempirical INDO CO formalism in the GC ensemble. In the case of the oxidized material we have collected the q_A figures for the symmetry adapted and symmetry nonadapted modifications with $\Delta z = 0$ Å as well as for the infinitesimal displacement $\Delta z = 0.001$ Å.

Atom	Unoxidized stack	Symmetry adapted $\Delta z = 0$ Å	Oxidized stack	
			Symmetry nonadapted $\Delta z = 0$ Å *	$\Delta z = 0.001$ Å
Mn	0.1305	0.2590	0.2140	0.1936
M̌n	0.1305	0.2590	0.3062	0.3305
C	−0.1659	−0.1440	−0.1442	−0.1445
Č	−0.1659	−0.1440	−0.1444	−0.1444
H	0.1398	0.1912	0.1926	0.1922
Ȟ	0.1398	0.1912	0.1920	0.1922

* The symmetry nonadapted solution corresponds to the variational minimum.

The electronic modifications accompanying the injection of holes can be analyzed via the atomic net charges q_A [128] in the unoxidized 1D material, the oxidized system with $\Delta z = 0$ Å as well as the $\Delta z = 0.001$ Å geometry (charged 1D chains) which are summarized in Table 1. The charge distribution in the unoxidized Mn(I) stack is symmetry adapted, i.e. identical q_A figures are predicted for the three atomic species (Mn, C and H) in the two halfs of the stacking-units. The HF minimum in the oxidized material is given by a spatially violated solution which leads to a reduction of the translation symmetry. The "suitable unit cell" corresponds to two MnCp fragments (in contrast to the neutral 1D column with $\Delta z = 0$ Å). The percentage charge separation between the two Mn sites (related to the net charge transfer from the Mn $3d_{z^2}$ regime) amounts to ca. 20% ($\Delta z = 0$ Å), i.e. 40% of the Mn electrons have been removed from one 3d center,

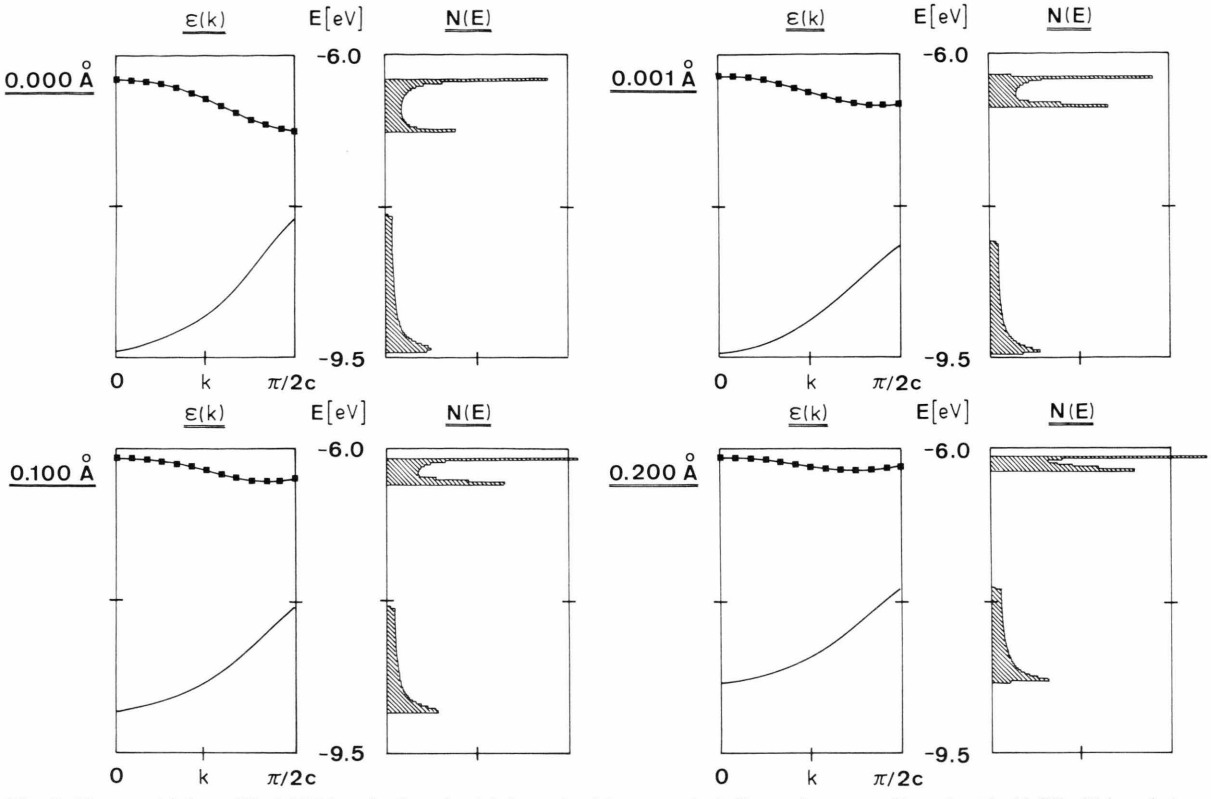

Fig. 5. The two highest filled HF bands (i.e. the highest doubly occupied dispersion as well as the "half-filled" band that is statistically occupied in the k-interval $0 \leqq k \leqq \pi/2c$, $\langle n_i \rangle_{GC} = 1$) and the density of states distributions, $N(E)$, of partly oxidized **1** in a 3.5 eV window. The $\varepsilon(k)$ and $N(E)$ diagrams are given for displacement coordinates $\Delta z = 0.0$ Å, 0.001 Å, 0.1 Å and 0.2 Å, respectively. The absolute positions of the HF bands have been shifted in order to match the one-electron energies of the unoxidized 1D chains. The two diagrams, $\varepsilon(k)$ and $N(E)$, associated with the $\Delta z = 0$ Å arrangement correspond to the symmetry nonadapted HF ground state of oxidized **1**. A common scale factor has been adopted to normalize the four $N(E)$ histograms; the energy grid used for the discrete sampling technique amounts to 0.025 eV. The "half-filled" bands of **1** are labeled by black squares.

60% are due to the second transition metal atom of the repeat-unit. The infinitesimal lattice relaxation of 0.001 Å allows for a sudden increase of Δq_{Mn} ($= q_{Mn} - \tilde{q}_{Mn}$). The ratio of the transferred charge is now 37% vs. 63%; nearly two third of the 3d electrons have been removed from one Mn center. The q_A numbers in Table 1 demonstrate furthermore important σ (and π) contributions from the ligand subspace in the oxidation process. The injected holes cause remarkable charge shifts at the H atoms in the cyclic ligands.

The net charges in Tab. 1 furthermore allow for the interpretation of two interesting theoretical aspects: a) The charge distribution in the two different sets of ligand atoms is nearly identical ($q_C \cong \tilde{q}_C$, $q_H \cong \tilde{q}_H$) in the oxidized polymer with $\Delta z = 0$ Å and $\Delta z = 0.001$ Å, respectively. Symmetry reductions within the Mn $3d_{z^2}$ subspace are not accompanied by electronic responses in the ligand framework. b) Extensive model calculations lead to the localization of a second, symmetry adapted HF solution in the oxidized Mn(I) material at $\Delta z = 0$ ($q_{Mn} = \tilde{q}_{Mn}$). This configuration lies ca. 6 kJ (per unit cell) above the mean-field ground state with different electronic populations at the two Mn centers. The symmetry adapted solution corresponds thus to a saddle-point in the allowed variational space.

The symmetry nonadapted hole-state properties of oxidized **1** (M-L-M solid) and the recently investigated [39] tetracyanonickelate (M-M stacking pattern) are comparatively summarized in Table 2. The transfer process in the Ni(II) material is prevailingly

Table 2. Comparison between the hole-state properties of partially oxidized $[(MnCp)_2]_\infty$ (investigated in the present contribution) and our previous results derived for the tetracyanonickelate(II) system, $\{[Ni(CN)_4^{2-}]_2^{+}\}_\infty$ (see [39]). The figures in the second column symbolize the channels (metal M, ligand L) involved in the injection process of the carriers (in %). The separation of the net charges Δq_M $(= q_M - \tilde{q}_M)$ is also summarized in the table. The charge transfer (in %) from the two transition metal atoms is given in the last column. These parameters are of course related to the localization properties of the hole-states (reference: %M in the second column). 100% corresponds to an exclusive transfer of 3d electrons from one site in the adopted repeat-units. The figure > 100% (i.e. 109%) in the Ni(II) backbone must be traced back to an electron transfer to the second Ni site that accompanies the ejection process. A negative value is thus found at the second 3d center. The computational results for **1** correspond to the 1D chain with the infinitesimal lattice relaxation (Δz = 0.001 Å).

1D System	Hole-state localization		Charge separation Δq_M 3d centers	Charge transfer from the two 3d centers (%)	
	%M	%L		M	$\tilde{M}$
$[(MnCp)_2^+]_\infty$	26	74	0.137	63	37
$\{[Ni(CN)_4^{2-}]_2^{+}\}_\infty$	73	27	0.868	109	−9

metal-centered (73% vs. 27% ligand mixtures) while large ligand contributions are predicted in the manganese derivative (26% vs. 74%). The charge separations (absolute values) between the 3d centers differ dramatically in the two 1D polymers (0.173 e vs. 0.868 e). The relative participation of the Mn centers to the net transfer in **1** is ca. 2/3 to 1/3, on one hand, an exclusive hole-transfer from one Ni site is diagnosed in the tetracyano Ni(II) system, on the other. The charge deficit at the oxidized Ni center is even enlarged via a superimposed electron transfer to the adjacent (unoxidized) 3d atoms.

The one-center potentials E_{A_0} (Mn, C, H) of the neutral and oxidized Mn poly-deckers (Δz = 0.001 Å in the charged system) are displayed in Figure 6. To relate these data to the theoretical findings derived for the $Ni(CN)_4^{2-}$ chain, also the latter one-center energies have been collected in this work (Figure 7). The one-center potentials of the organic ligands are almost identical in the two modifications of **1** (Figure 6). The "translation symmetry" with respect to the E_{A_0} elements of C and H is not lowered ($E_{C_0} \cong \tilde{E}_{C_0}$, $E_{H_0} \cong \tilde{E}_{H_0}$).

The E_{A_0} terms at the two Mn atoms, however, differ by ca. 2.5 eV. The upper E_{Mn_0} values are of course associated to the "oxidized Mn centers", i.e. to the 3d centers with the larger charge deficit. The alternating arrangement of the two Mn species embedded into an averaged ligand potential is shown at the bottom of Figure 6. The drawings in

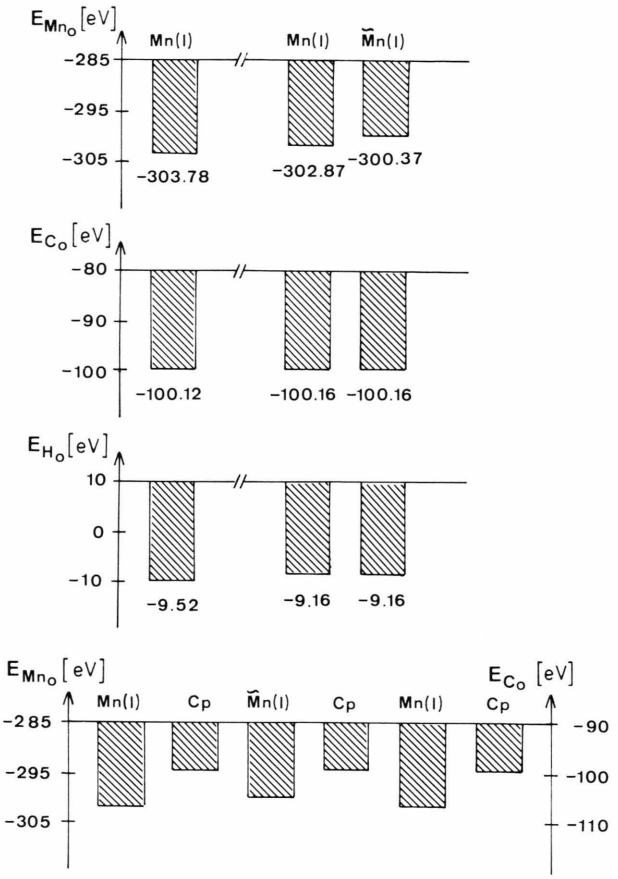

Fig. 6. Schematic representation of the one-center potentials E_{A_0} of Mn, C and H in the unoxidized poly-decker **1** (lhs.) as well as in the partially oxidized material (rhs.); the latter numbers are associated to the 1D column with the infinitesimal Δz = 0.001 Å deformation. The ligand potentials (C and H) in the oxidized backbone conserve the original translation symmetry of the neutral chain, i.e. all Cp units are electronically equivalent. The Mn potentials at the two 3d sites in a given cell differ by 2.5 eV in the 1D column with injected holes. The energetic separation $E_{Mn_0}/\tilde{E}_{Mn_0}$ in the oxidized 1D system with symmetric nuclear coordinates amounts to ca. 1.5 eV (spatially broken solution). The H admixtures to the a_1 hole-state of **1** lead to an E_{H_0} shift of ca. 0.35 eV as response to the removal process ($\tilde{E}_{H_0}$: − 9.52 eV, neutral 1D chain, E_{H_0}: − 9.11 eV, oxidized chain). The modifications of the mono-center potentials at the carbon sites in the two states are significantly smaller. At the bottom of the figure we have schematized the alternating arrangement of the Mn centers (E_{Mn_0} and $\tilde{E}_{Mn_0}$, respectively) embedded into an averaged ligand potential (Cp). Only the E_{A_0} terms of the C atoms are displayed in this simplified representation (A = C).

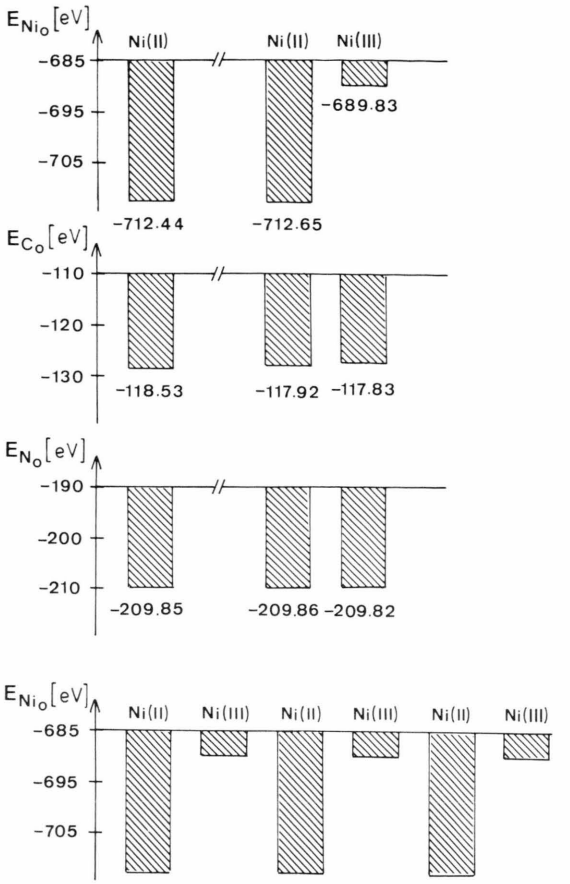

Fig. 7. Schematic representation of the various one-center energies E_{A_0} (A = Ni, C, N) of the unoxidized $Ni(CN)_4^{2-}$ solid (lhs.) and the oxidized 1D material (rhs.). The holes in the 1D backbones are prevailingly confined to the Ni $3d_{z^2}$ spine. The one-center energies at the two transition metal atoms per unit cell differ by almost 23 eV (strong valence trapping). The charge reorganizations at the 3d centers are accompanied by small polarization effects in the CN ligands. The removal process at the central atoms leads to an E_{C_0} shift of ca. 0.6 eV; the changes at the N atoms are negligibly small. The alternating arrangement of Ni(II) and Ni(III) functions in the partly oxidized tetracyano system is displayed at the bottom of the figure.

Fig. 7 indicate the significantly enlarged separation of the E_{Ni_0} terms (Ni(II) vs. Ni(III)) in the tetracyano stack. The two potentials differ by more than 23 eV. This strong valence trapping, however, is accompanied by a perceptible polarization in the ligand framework.

The arrangement of the E_{A_0} potentials in oxidized **1** shows a formal superposition of two translational symmetries in the one-dimensional material. A simplified real-space representation based on the calculated atomic net charges q_A and one-center energies E_{A_0} is given in Figure 8. The organic π ligands form one sublattice with a periodicity identical with the interplanar separation between the Cp moieties (i.e. c) while the Mn sites belong to a second sublattice with a doubled unit cell (i.e $2c$) and a bisected Brillouin zone.

A graphic representation of the atomic net charges at the two Mn sites per unit cell is given in Fig. 9 for the partly oxidized 1D system in a Δz interval between $0 \leqq \Delta z \leqq 0.2$ Å. The charge separation between the transition metal centers of the unoxidized backbone amounts to only 0.014 e ($\Delta z = 0.2$ Å) and is thus negligibly small in comparison to Δq_{Mn} of th oxidized stack. Relative mean-field energies (normalized to one unit cell) have been collected in Fig. 10 in the above mentioned Δz area $0 \leqq \Delta z \leqq 0.2$ Å. The plotted ΔE figures are defined in (31) and (32), respectively.

$$\Delta E_{TOT}(z) = E_{TOT}(\Delta z = 0) - E_{TOT}(\Delta z), \quad (31)$$

I = unoxidized polymer,

II = partly oxidized polymer,

$$\Delta E(z) = \Delta E^{II}_{TOT}(z) - \Delta E^{I}_{TOT}(z). \quad (32)$$

ΔE corresponds to the gain ($\Delta E < 0$) or loss ($\Delta E > 0$) in energy associated with the lattice deformation Δz in the charged polymer compared with

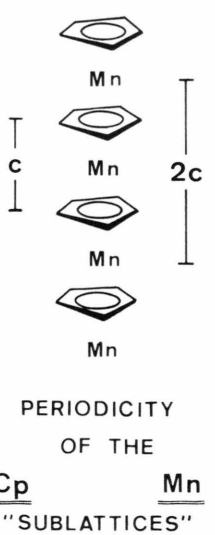

Fig. 8. Periodicity of the Cp (i.e. c) and Mn (i.e. $2c$) sublattices in partly oxidized **1**. c is the interplanar spacing between adjacent cyclopentadienyl ligands or Mn atoms, respectively.

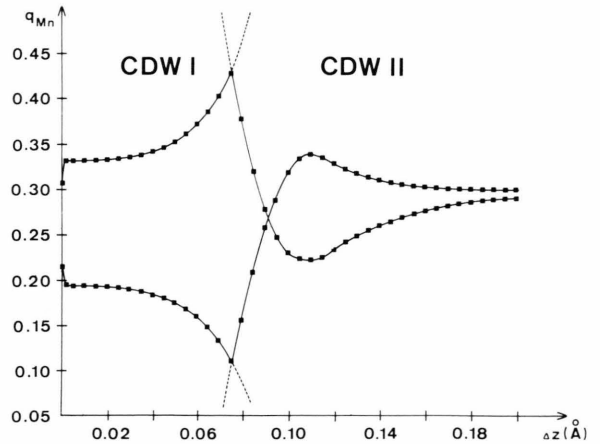

Fig. 9. Net charges q_{Mn} of the transition metal sites of partly oxidized **1** as a function of the displacement coordinate Δz. The "sudden" character of the symmetry violation for infinitesimal Δz amplitudes is seen on the extreme left of the q_{Mn} plot. CDW I and CDW II have been used to label the two charge density wave solutions in the oxidized 1D material.

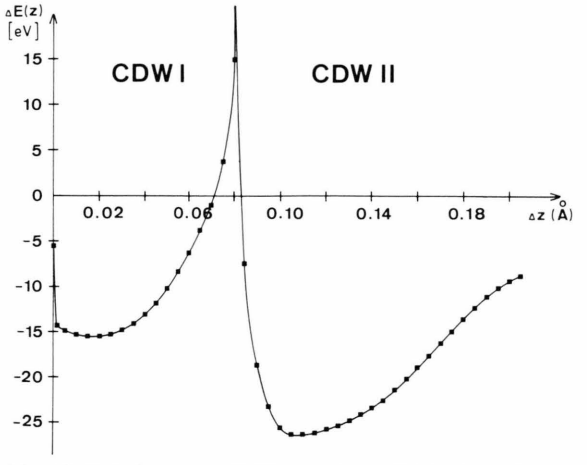

Fig. 10. Relative mean-field energies $\Delta E(z)$ of partly oxidized **1** as a function of the displacement coordinate Δz. The HF energies of the uncharged 1D polymer have been employed as internal standard for the $\Delta E(z)$ curves. $\Delta E(z)$ is defined in (32). CDW I and CDW II are the two charge density wave regimes observed in the variational crystal orbital approach (see Fig. 9).

the neutral parent which has been used as internal standard. The lattice mode thus allows for a stabilization of the cationic chain (compared to uncharged **1**) for ΔE parameters < 0 while a destabilization is characterized by $\Delta E > 0$.

The remarkable charge separation between the transition metal centers Δq_{Mn} for infinitesimal lattice deformations Δz already has been discussed in connection with Table 1. The "sudden" character of the q_{Mn} and ΔE numbers in the vicinity of the symmetric arrangement is easily recognized both in Figs. 9 and 10. The imbalance of the electronic population at the Mn centers is then continuously enlarged in the interval $0 \leqq \Delta z \leqq 0.07$ Å (Figure 9). Figure 10 shows complimentarily that this lattice deformation is stabilized in the charged polydecker. The difference between the q_A parameters associated with the two types of carbon (C/C̃) and hydrogen (H/H̃) atoms is once again negligibly small. A further Δz elongation, however, causes a retrograde Δq_{Mn} variation, i.e. the charge separation between the Mn sites is strongly reduced in a rather narrow Δz interval of 0.01 Å. The q_{Mn} plot of Fig. 9 verifies that the electronic population is even switched. A "net hole" migration from the Mn sites with longer metal-ligand bonds to the 3d centers with shorter MnC distances is observed. Such a Δq_{Mn} variation corresponds to an "electronic" phase transition [65] between two different electronic configurations. The nature of this transition is clearly seen in Fig. 10 where two pronounced $\Delta E(z)$ minima are separated by a barrier at $\Delta z \cong 0.08$ Å.

In order to rationalize the physical origin of the symmetry reduction in charged **1** as well as to understand the computational results displayed in Figs. 9 and 10 we have decomposed the two-center energies (intracell pairs) $E_{A_0B_0}$ of the CC, CH and MnC bonds and the MnMn pair into the above mentioned fragments $E^{RES}_{A_0B_0}$, $E^{EX}_{A_0B_0}$ and $E^{COU}_{A_0B_0}$, respectively (Table 3). The CC and CH couples form strongly covalent bonds with interaction potentials

Table 3. Energy fragmentation of the CC, CH, MnC and MnM̃n couples (intracell pairs) of the uncharged Mn(I) polymer **1** with $\Delta z = 0$ Å according to the semiempirical crystal orbital approach. The net two-center energies $E_{A_0B_0}$ have been divided into resonance ($E^{RES}_{A_0B_0}$), exchange ($E^{EX}_{A_0B_0}$) and electrostatic Coulomb potentials ($E^{COU}_{A_0B_0}$). All values in eV.

Two-center couple	$E^{RES}_{A_0B_0}$	$E^{EX}_{A_0B_0}$	$E^{COU}_{A_0B_0}$	$E_{A_0B_0}$
CC	−20.833	−4.316	−2.687	−27.836
CH	−15.648	−4.395	−0.749	−20.791
MnC	− 4.009	−0.899	−0.547	− 5.454
MnM̃n	− 0.260	−0.146	0.092	− 0.314

that are in the first place determined by the kinetic energy operator. This behaviour is of course expected for typical ligand bonds. On the other hand, also the mutual coupling between the Mn sites and the C atoms is controlled by the one-electron part of the crystal Hamiltonian. The magnitude of the MnC potential is reduced by a factor 4–5 in comparison to $E_{C_0H_0}$ and $E_{C_0C_0}$, respectively, but the relative composition ($E^{RES}_{A_0B_0}$, $E^{EX}_{A_0B_0}$ and $E^{COU}_{A_0B_0}$) of different two-center interaction energies is roughly comparable (see below).

	$E^{RES}_{A_0B_0}$	$E^{EX}_{A_0B_0}$	$E^{COU}_{A_0B_0}$	(in %)
CC	74.8	15.5	9.7	
CH	75.3	21.1	3.6	
MnC	73.5	16.5	10.0	

These numbers differ significantly from the interaction energy between the two Mn atoms in the employed unit cell which is small (– 0.314 eV) in comparison to the $E_{A_0B_0}$ elements derived for the ligand-ligand and metal-ligand bonds. The kinetic hopping terms and the exchange part are slightly stabilizing while the Coulomb contribution is repulsive.

The calculated $E^{RES}_{Mn_0\tilde{M}n_0}$, $E^{EX}_{Mn_0\tilde{M}n_0}$ and $E^{COU}_{Mn_0\tilde{M}n_0}$ numbers demonstrate immediately the inadequacy of symmetry adapted solutions for hole-state wave functions disposing of significant Mn 3d amplitudes. The mutual coupling strength between the transition metal sites is so small that the wave functions are "strongly localized" at the Mn centers. In the case of an electronically isolated ... Mn $\tilde{M}$n ... arrangement (absence of bridging ligand functions) extremely strong electronic rearrangement processes would be expected that conduct to spatially violated holes. These incoherent scattering events allow for a condensation of trapped valences with $q_{Mn} \neq \tilde{q}_{Mn}$ and $|q_{Mn} - \tilde{q}_{Mn}| \gg 0$. The reorganization events in the Mn 3d subspace guarantee that important spatial correlation effects (left-right correlations) are taken into account in a variational approach that is nevertheless restricted to the mean-field approximation (with reduced translation symmetries). Such pronounced left-right correlations between the metal centers indeed have been diagnosed in the above mentioned partly oxidized tetracyanonickelate(II) system which belongs to the M-M solids [39]. The relative importance of the kinetic energy operator (favouring spatially nonviolated hole-state wave functions) and the two-electron part of the tight-binding Hamiltonian (i.e. energy gain via incoherent reorganization processes), however, is modified in **1** by means of the bridging Cp ligands which contribute to highly covalent metal-ligand bonds. The Mn-Cp admixtures to the CO microstates of the highest filled "Mn $3d_{z^2}$ band" catagonize a possible reduction of the translation symmetry in the charged polymer. The observed Δq_{Mn} values of **1** (which are significantly smaller than the theoretically determined charge separation between the Ni sites in oxidized $Ni(CN)_4^{2-}$) are thus the optimum compromise between the Mn $\tilde{M}$n interaction ($E_{Mn_0\tilde{M}n_0}$) which favours the formation of trapped valences and the $E_{Mn_0C_0}$ energy stabilizing coherent hole-states. The localization properties of the highest occupied a_1 band in the uncharged Mn(I) material (> 70% Mn $3d_{z^2}$ amplitudes) as well as in the oxidized stack (≅ 26%) suggest a strong imbalance between the driving forces due to $E_{Mn_0\tilde{M}n_0}$, on one hand, and $E_{Mn_0C_0}$, on the other (see (33)) thus demanding an increase of the ligand admixtures in the corresponding hole-state wave function. The influence of the latter interaction mechanism is thus enhanced.

$$|E_{Mn_0\tilde{M}n_0}|_{INCOH} \gg |E_{Mn_0C_0}|_{COH}\,, \qquad (33)$$

(IN)COH: (in)coherent phenomena in the 1D column.

The symmetry broken hole-state wave functions in **1** within the employed variational degrees of freedom are charge density waves (CDW). The analysis of the bond-order matrices shows that the CDW solutions are both characterized by diagonal and off-diagonal elements [129]. The off-diagonal CDW contributions must be traced back to the ligand admixtures encountered in the CO wave functions of the cationic hole-states. It is well-known that (off-diagonal) CDW solutions are often coupled to displacements of the nuclear framework into the direction of the instability if the Hellmann-Feynman force-theorem is fulfilled for the one-dimensional arrangement. These non-zero forces are obviously responsible for the $\Delta E(z)$ variation displayed in Fig. 10 with an energy minimum encountered for $\Delta z \neq 0$ (CDW I region). A second charge density

wave solution, CDW II, is then stabilized if Δz is furthermore enlarged; this configuration is characterized due to the above mentioned switch of the charge distribution at the Mn centers (see Figs. 9 and 10).

The necessary computational restrictions focused our analysis to the most simple oxidation process, i.e. to a charge transfer where one electron has been removed from each second MnCp moiety. On the basis of the theoretical insight into the physical nature of these hole-states it is however possible to extend the present results from a specific occupation pattern to the manifold of possible filling schemes. This extrapolation can be applied to all band occupancies where the CO microstates from the Γ- to the X-points are statistically filled by a fractional number of electrons defined by $\langle n_i \rangle_{GC}$. Commensurate CDW solutions within three, four, five, six, etc. stacking units S_n ($n = 3, 4, 5, 6, \ldots$) are expected for occupancies such as 1/3, 1/4, 1/5 and 1/6, respectively ($\langle n_i \rangle_{GC} = 2/3$, 1/2, 2/5 and 1/3, respectively as $\langle n_{i,\max} \rangle_{GC} = 2$). The probable electronic responses to such electronic configurations are violations of the translation symmetries within three, four, five or six molecular building blocks S leading to 1D materials with "unit cells" of the stoichiometry $(S_3)_\infty$, $(S_4)_\infty$, $(S_5)_\infty$, and $(S_6)_\infty$. The spatial symmetry violations within these moieties simulate always transitions from inadequate coherent MO structures to one of the possible VB-type wave functions. Incommensurate CDW solutions, on the other hand, are expected for population schemes that deviate from the aforementioned simple fractions between the degree of oxidation and the number of molecular stacking units.

Two additional theoretical shortcomings of the present idealized approach have to be taken into account in transferring the findings to "real crystals" (even at $T = 0\,\mathrm{K}$) or to finite temperatures ($T \neq 0$). In real solids with imperfections, impurities, surface effects or random potentials the formation of domain structures or finite clusters (see Fig. 11) always has to be taken into account. Periodic boundary conditions are not longer valid to analyze the electronic structures of these materials. Suitable theoretical approaches for such aperiodic structures are based on interrupted strand models [130] that are closely related to popular particle in the box problems as well as to computational methods based on the coherent potential approximation (CPA) [131].

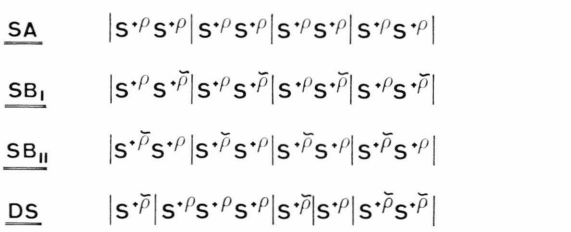

Fig. 11. Schematic representation of various possible oxidation states of the one-dimensional solid S_∞. SA symbolizes the symmetry adapted phase with electronically equivalent lattice sites S within a given unit cell. SB_I and SB_{II} are the two degenerate solutions with reduced translation symmetries leading to $+\varrho \neq +\tilde{\varrho}$. The last representation DS corresponds to domain or cluster structures containing finite areas where either the $+\varrho$ states or the $+\tilde{\varrho}$ populations, respectively, are found. Cyclic boundary conditions, of course, are nonvalid in the latter case.

The above mentioned E figures are also irrelevant in idealized crystals for finite temperatures $T \neq 0$ where the thermodynamic properties of the solid state ensembles are determined by the free energy G, (34), which is given by the (HF) contribution E and the entropy term TS.

$$G = E - TS\,. \tag{34}$$

A statistical definition of the entropy factor TS is displayed in (35) by means of the probability W which is the number of different ways to distribute the two types of stacking units $S^{+\varrho}$ and $S^{+\tilde{\varrho}}$, respectively, over the one-dimensional array ($+\varrho$, $+\tilde{\varrho}$: degree of oxidation) [132].

$$TS = Tk \cdot \ln W\,. \tag{35}$$

It is clear that $\ln W$ with $W = 2$ which is associated with the strictly alternating structures (see Fig. 11) $\ldots S^{+\varrho} S^{+\tilde{\varrho}} S^{+\varrho} S^{+\tilde{\varrho}} \ldots$ and $\ldots S^{+\tilde{\varrho}} S^{+\varrho} S^{+\tilde{\varrho}} S^{+\varrho} \ldots$ is negligibly small in comparison to $\ln W$ derived for all possible permutations of $S^{+\varrho}$ and $S^{+\tilde{\varrho}}$ over N lattice sites where N is of the order of 10^{23} (Avogadro's number).

$$W = \binom{N}{(N/2)} = \frac{N!}{[(N/2)!]^2} \cong \frac{(N/e)^N}{(N/2e)^N} = 2^N\,, \tag{36}$$

$$TS \cong Tk \cdot \ln (2^N)\,. \tag{37}$$

Domain structures with random distributions of $S^{+\varrho}$ and $S^{+\tilde{\varrho}}$ are thus always favoured in comparison to the strictly alternating arrangement above a characteristic temperature T_D. The magnitude of T_D depends obviously on the electronic stabilization

measured by E, i.e. the possible gain in energy (left-right correlations) due to violations of spatial symmetries. In the present calculations we have derived $E_{max} \cong 15$ kJ for the partly oxidized poly-decker **1** in a slightly displaced structure. It is of course an extremely difficult task to make a reliable estimation for an averaged E parameter $\bar{E}$ that is a measure for the energy reduction due to the transition from a common oxidation state with $S^{+\varrho_{av}}$ into a macroscopic ensemble $S^{+\varrho}$ and $S^{+\tilde{\varrho}}$ with arbitrary arrangements of the two objects. The magnitude of $\bar{E}$ is in any case restricted due to the inequivalence expressed in (38).

$$0 \leqq |\bar{E}| \ll |\bar{E}_{max}| \,. \tag{38}$$

The "transition temperature" T_D is then defined in (39).

$$T_D = \frac{E_{max} - \bar{E}}{k \ln 2 - k \ln (2^N)} \cong \frac{E_{max} - \bar{E}}{k \ln (2^N)} \,. \tag{39}$$

The energy denominator $k \ln (2^N)$ is responsible for T_D parameters in the infinitesimal neighborhood of $T = 0$. The temperature domain T_D of a three-dimensional ordering is however enlarged if interchain interactions (e.g., Coulomb forces, Van der Waals coupling or Josephson tunneling) are taken into account [133].

6. Conclusions

The electronic structure of the one-dimensional sandwich compound **1** has been studied in the uncharged ground state and in a partly oxidized modification where one electron has been removed from each second MnCp moiety. In order to analyze possible violations of translation symmetries in the charged 1D column (separated from spin-dependent phenomena, antiferromagnetic sublattices) we have employed a statistical ensemble-averaged crystal Hamiltonian based on the grand canonical ensemble. The mean-field ground state of the oxidized material is given by a solution with an alternating arrangement of Mn atoms in different oxidation states embedded into an averaged ligand potential with a periodicity that exceeds the translation symmetry with respect to the 3d centers by a factor of 2. A symmetry adapted solution with $q_{Mn} = \tilde{q}_{Mn}$ corresponds to a maximum in HF space. The reduction of the spatial symmetry between the translation metal centers has its origin in the weak coupling between the 3d atoms and the (relative) small ligand amplitudes in the highest filled band of **1**. The weak MnMn interactions cause strong left-right correlations that are accompanied by the aforementioned reduction of the spatial symmetry. This symmetry breaking simulates a transition from the "inadequate MO description" to one of the possible "VB structures". The spatial violation with respect to the Mn spine, however, is hampered due to the ligand admixtures encountered in the valence band of (unoxidized) **1**. The coupling mechanism between Mn and the C atoms in the fivemembered π ligands is highly covalent and favoures the formation of "broad" holes via a reduction of the kinetic energy. The hole-state properties of M-M solids, on one hand, and M-L-M chains, on the other, thus show significant differences. The ligand moieties in the former 1D materials can be regarded as a "matrix" (with respect to the 3d electrons of the central sites) which prevents close contacts (i.e. strong interactions) between the transition metal sites. The electronic structure in the 3d subspace of these materials is therefore not unlike to the physical conditions encountered in the idealized Wigner lattice in the low-density limit. The creation of holes within the 3d regime is always accompanied by strong incoherent reorganization processes (electronic correlations and relaxations) leading to large charge separations between the central atoms. Comparable Δq_M numbers in M-L-M systems are prevented due to the influence of the bridging groups L which allow for the reduction of the kinetic energy via the formation of delocalized holes. The observed charge separation in the oxidized poly-decker **1** is thus an optimum compromise between the "localized (3d) holes" in extended M-M columns, on one hand, and "delocalized holes" in materials with broad dispersion curves (several eV), on the other.

We believe that the perturbation of the translational symmetry is not a failure of the employed mean-field approximation, but corresponds to a "physically reliable" description of the partly oxidized modification of **1**. This conclusion is supported due to the theoretical findings derived in SCF investigations on weakly coupled cationic complexes of 3d metals as well as tight-binding investigations of Mott insulators. The reduction of the translation symmetry in **1** is of course also associated with the breakdown of the ergodic behaviour [134, 135], a

general phenomenon in condensed matter physics (e.g., Ising ferromagnets, spin glasses). Simple arguments have been derived suggesting that the observed symmetry violations simulate a transition from a perfectly ergodic state to an arrangement with broken ergodicity whose time-dependence (propagation of holes of electrons) is accessible to experimental measurements provided that the theoretical and experimental "time windows" coincide.

Acknowledgements

This work has been supported by the Stiftung Volkswagenwerk. The author wants to express his thanks to Prof. P. Fulde and Dipl. Phys. F. Pfirsch for useful discussions and to Dr. W. Borrmann for critically reading the manuscript. The assistance of Mrs. I. Grimmer in typing the manuscript is also gratefully acknowledged.

[1] H. J. Keller (ed.), Chemistry and Physics of One Dimensional Metals, Plenum Press, New York 1978; J. T. Devresse, R. P. Evrard, and V. E. van Doren (ed.), Highly Conducting One-Dimensional Solids, Plenum Press, New York 1979.
[2] D. B. Brown (ed.), Mixed Valence Compounds, D. Reidel Publ. Co., Dordrecht-Boston 1980; W. A. Hatfield (ed.), Molecular Metals, Plenum Press, New York 1980; L. Alcacér (ed.), The Physics and Chemistry of Low Dimensional Solids, D. Reidel Publ. Co., Dordrecht-Boston 1980.
[3] J. S. Miller (ed.), Extended Linear Chain Compounds, Plenum Press, New York 1982.
[4] M. Hanack and G. Pawlowski, Naturwiss. **69,** 266 (1982); M. Hanack, Chimia **37,** 238 (1983).
[5] J. A. Ibers, L. J. Pace, J. Martinsen, and B. M. Hoffman, Struct. Bonding **50,** 1 (1982); B. M. Hoffman and J. A. Ibers, Acc. Chem. Res. **16,** 15 (1983).
[6] H. Endres, H. J. Keller, R. Lehmann, A. Poveda, H. H. Rupp, and H. van de Sand, Z. Naturforsch. **32b,** 516 (1977); H. J. Keller, in: Mixed Valence Compounds, D. B. Brown (ed.), D. Reidel Publ. Co., Dordrecht-Boston, 1980.
[7] J. Hubbard, Proc. Roy. Soc. London **A276,** 238 (1963); **A277,** 237 (1963); **A281,** 401 (1964).
[8] Z. G. Soos, Ann. Rev. Phys. Chem. **25,** 121 (1974); Z. G. Soos and D. J. Klein, in: Molecular Association, R. Foster (ed.), Academic Press, New York 1975; J. B. Torrance, Acc. Chem. Res. **12,** 79 (1979).
[9] B. M. Hoffman, T. E. Phillips, and Z. G. Soos, Solid State Commun. **33,** 51 (1980); T. E. Phillips, R. P. Scaringe, B. M. Hoffman, and J. A. Ibers, J. Amer. Chem. Soc. **102,** 3435 (1980).
[10] J. Martinsen, L. J. Pace, T. E. Phillips, B. M. Hoffman, and J. A. Ibers, J. Amer. Chem. Soc. **104,** 83 (1982).
[11] L. J. Pace, J. Martinsen, A. Ulman, B. M. Hoffman, and J. A. Ibers, J. Amer. Chem. Soc. **105,** 2612 (1983).
[12] P. Csavinszky, in: Quantum Theory of Polymers, J. M. André, J. Delhalle, and J. Ladik (ed.), D. Reidel Publ. Co., Dordrecht-Boston 1978.
[13] T. E. Peacock and R. McWeeny, Proc. Phys. Soc. London **74,** 385 (1969); G. del Re, J. Ladik, and G. Biczó, Phys. Rev. **155,** 997 (1967); J. M. André, L. Gouverneur, and G. Leroy, Int. J. Quantum Chem. **1,** 997 (1967).
[14] J. Ladik and S. Suhai, in: Molecular Interactions, W. J. Orville-Thomas and H. Ratajack (ed.), Wiley Interscience, New York 1980; J. Ladik and S. Suhai, in: Theoretical Chemistry, Vol. 4; C. Thomson (ed.), Roy. Soc. Chem. London 1981; M. Kertész, Adv. Quantum Chem. **15,** 161 (1982).
[15] S. T. Pantelides, D. J. Mickish, and A. B. Kunz, Phys. Rev. **B10,** 2602 (1974).
[16] A. B. Kunz and D. L. Klein, Phys. Rev. **B17,** 4614 (1975); A. B. Kunz, Phys. Rev. **B26,** 2056 (1982).
[17] S. Suhai, in: Quantum Theory of Polymers, J. M. André, J. Delhalle, and J. Ladik (ed.), D. Reidel Publ. Co., Dordrecht-Boston 1978.
[18] A. Miller and A. Abrahams, Phys. Rev. **120,** 745 (1960); N. F. Mott and W. D. Twose, Adv. Phys. **10,** 107 (1961).
[19] T. Holstein, Ann. Phys. **8,** 343 (1959).
[20] J. T. Devresse (ed.), Polarons in Ionic Crystals and Polar Semiconductors, North-Holland Publ. Co., Amsterdam 1972.
[21] D. Emin, Adv. Phys. **22,** 57 (1973); D. Emin, in: Electronic and Structural Properties of Amorphous Semiconductors, P. G. le Comber and J. Mort (ed.), Academic Press, London 1973.
[22] M. Pollack, J. Non-Crystalline Solids **11,** 1 (1972).
[23] R. Kopelman, E. M. Momberg, F. W. Ochs, and P. N. Prasad, J. Chem. Phys. **62,** 292 (1975); A. Blumen and R. Silbey, J. Chem. Phys. **70,** 3707 (1979).
[24] M. C. Böhm, Theor. Chim. Acta **62,** 351 (1983).
[25] M. C. Böhm and R. Gleiter, Theor. Chim. Acta **59,** 127, 153 (1981).
[26] M. C. Böhm, Phys. Letters **93A,** 205 (1983); M. C. Böhm, J. Chem. Phys. **80,** 2704 (1984).
[27] M. C. Böhm, Chem. Phys. **76,** 1 (1983).
[28] M. C. Böhm, Z. Naturforsch. **39a,** 223 (1984).
[29] M. C. Böhm, Theor. Chim. Acta **62,** 373 (1983); M. C. Böhm, Z. Phys. Chem. (Neue Folge) **133,** 25 (1982); M. C. Böhm, Physica **124B,** 203 (1984).
[30] M. C. Böhm, Physica **122B,** 302 (1983).
[31] M. C. Böhm, J. Phys. C: Solid State Phys. **16,** 1631 (1983).
[32] M. C. Böhm, Solid State Commun. **45,** 117 (1983); M. C. Böhm, Int. J. Quantum Chem. **25,** 817 (1984).
[33] M. C. Böhm, Phys. Letters **94A,** 371 (1983); M. C. Böhm, J. Phys. C: Solid State Phys. **17,** 2091 (1984).
[34] M. C. Böhm, Phys. Rev. **B28,** 6914 (1983).
[35] M. C. Böhm, Phys. Letters **102A,** 121 (1984); M. C. Böhm, Chem. Phys. Letters **107,** 322 (1984).
[36] J. Hubbard, Phys. Rev. **B17,** 494 (1978); J. B. Torrance, Phys. Rev. **B17,** 3099 (1978).
[37] M. Weger and H. Gutfreund, Solid State Commun. **32,** 1259 (1979); S. Huizinga, J. Kommandeur, G. A. Sawatzky, B. T. Thole, K. Kopinga, W. J. M. de Jonge, and J. Roos, Phys. Rev. **B19,** 4723 (1979).
[38] R. W. White and T. H. Geballe, in: Long Range Order in Solids, Solid State Phys. Suppl. **15,** H. Ehrenreich, F. Seitz, and D. Turnbull (ed.), Academic Press, New York 1979.

[39] M. C. Böhm, J. Chem. Phys., in press.
[40] W. Siebert, Adv. Organomet. Chem. **18,** 301 (1980) and references cited therein; W. Siebert, in: Transition Metal Chemistry, A. Müller and E. Diemann (ed.), Verlag Chemie, Weinheim 1981, and references cited therein.
[41] J. Edwin, M. Bochmann, M. C. Böhm, D. E. Brennan, W. E. Geiger, C. Krüger, J. Pebler, H. Pritzkow, W. Siebert, W. Swiridoff, H. Wadepohl, J. Weiss, and U. Zenneck, J. Amer. Chem. Soc. **105,** 2582 (1983).
[42] M. Elian and R. Hoffmann, Inorg. Chem. **14,** 365 (1975); M. Elian, M. M. L. Chen, D. M. P. Mingos, and R. Hoffmann, Inorg. Chem. **15,** 1148 (1976).
[43] J. W. Lauher, M. Elian, R. Summerville, and R. Hoffmann, J. Amer. Chem. Soc. **98,** 3219 (1976).
[44] M. C. Böhm, Ber. Bunsenges. Phys. Chem. **85,** 755 (1981).
[45] S. F. Abdulnur, J. Lindenberg, Y. Öhrn, and P. W. Thulstrup, Phys. Rev. **A6,** 889 (1972).
[46] P. Jørgensen, J. Chem. Phys. **57,** 4884 (1972).
[47] J. Linderberg and Y. Öhrn, Propagators in Quantum Chemistry, Academic Press, London 1973.
[48] M. C. Böhm, Z. Phys. B: Condensed Matter **56,** 99 (1984).
[49] D. J. Thouless, Nucl. Phys. **21,** 255 (1960); D. J. Thouless, The Quantum Mechanics of Many-Body Systems, Academic Press, New York 1961.
[50] J. Čižek and J. Paldus, J. Chem. Phys. **47,** 3976 (1967).
[51] H. Fukutome, Int. J. Quantum Chem. **20,** 955 (1981).
[52] P.-O. Löwdin, in: Quantum Theory of Atoms, Molecules, and the Solid State, P.-O. Löwdin (ed.), Academic Press, New York 1966.
[53] P.-O. Löwdin, Rev. Mod. Phys. **183,** 68 (1963); P.-O. Löwdin, Adv. Chem. Phys. **14,** 283 (1969).
[54] M. C. Böhm, R. Gleiter, F. Delgado-Pena, and D. O. Cowan, Inorg. Chem. **19,** 1081 (1980); M. C. Böhm, R. Gleiter, F. Delgado-Pena, and D. O. Cowan, J. Chem. Phys. **79,** 1154 (1983).
[55] T. H. Upton and W. A. Goddard III, J. Amer. Chem. Soc. **100,** 5659 (1978).
[56] H. van Dam, J. Stufkens, A. Oskam, M. Doran, and I. H. Hillier, J. Electron Spectrosc. Relat. Phenom. **21,** 47 (1980); H. van Dam, J. N. Louwen, A. Oskam, M. Doran, and I. H. Hillier, J. Electron Spectrosc. Relat. Phenom. **21,** 57 (1980).
[57] P. A. Cox, M. Benard, and A. Veillard, Chem. Phys. Letters **87,** 159 (1982).
[58] D. Post and E. J. Baerends, Chem. Phys. Letters **87,** 176 (1982); R. P. Messmer, T. C. Caves, and C. M. Kao, Chem. Phys. Letters **90,** 296 (1982).
[59] M. D. Newton, Chem. Phys. Letters **90,** 291 (1982).
[60] M. Benard, Theor. Chim. Acta **61,** 379 (1982).
[61] M. Benard, Chem. Phys. Letters **96,** 183 (1983).
[62] P. T. Chesky and M. B. Hall, Inorg. Chem. **22,** 2998 (1983).
[63] J. Paldus and J. Čižek, Chem. Phys. Letters **3,** 1 (1969); J. Paldus and J. Čižek, J. Chem. Phys. **52,** 2919 (1970).
[64] M. C. Böhm, Theor. Chim. Acta **60,** 233 (1981); M. C. Böhm, Mol. Phys. **46,** 255 (1982).
[65] M. C. Böhm, J. Phys. B: At. Mol. Phys. **16,** L397 (1983); M. C. Böhm, Int. J. Quantum Chem. **24,** 185 (1983).
[66] L. Noodleman and J. G. Norman, J. Chem. Phys. **70,** 4093 (1979); M. Bernard, J. Chem. Phys. **71,** 2546 (1979).
[67] C. Herring, in: Magnetism, Vol. **4,** G. T. Rado and H. Suhl (ed.), Academic Press, New York 1966.
[68] J.-L. Calais, Int. J. Quantum Chem. **S11,** 547 (1977).
[69] R. Peierls, Quantum Theory of Solids, Clarendon Press, London 1955.
[70] A. Denis, J. Langlet, and J. P. Malrieu, Theor. Chim. Acta **38,** 49 (1975).
[71] W. H. E. Schwarz and T. C. Chang, Int. J. Quantum Chem. **S10,** 91 (1976).
[72] M. C. Böhm, Theor. Chim. Acta **60,** 455 (1982).
[73] N. F. Mott, Can. J. Phys. **34,** 1356 (1956).
[74] J. B. Goodenough, Magnetism and the Chemical Bond, Interscience Publishers, New York 1963.
[75] M. B. Robin and P. Day, Adv. Inorg. Chem. and Radiochem. **10,** 247 (1967).
[76] P. Day, in: Low-Dimensional Cooperative Phenomena, H. J. Keller (ed.), Plenum Press, New York 1975; P. Day, Ann. N.Y. Acad. Sci. **313,** 9 (1978).
[77] P. Day, in: The Physics and Chemistry of Low-Dimensional Solids, L. Alcacér (ed.), D. Reidel Publ. Co., Dordrecht-Boston 1980; P. Day, in: Mixed Valence Compounds, D. B. Brown (ed.), D. Reidel Publ. Co., Dordrecht-Boston 1980.
[78] M.-H. Whangbo, J. Chem. Phys. **70,** 4963 (1979); M.-H. Whangbo, M. J. Foshee, and R. Hoffmann, Inorg. Chem. **19,** 1723 (1980).
[79] M.-H. Whangbo, Acc. Chem. Res. **16,** 95 (1983).
[80] N. F. Mott, Phil. Mag. **6,** 281 (1961); N. F. Mott, Metal-Insulator Transitions, Taylor and Francis, London 1974.
[81] D. Alder, in: Solid State Phys. Vol. **21,** H. Ehrenreich, F. Seitz, and D. Turnbull (ed.), Academic Press, New York 1968; D. Adler and J. Feinleib, Phys. Rev. **B2,** 2112 (1970).
[82] B. H. Brandow, Int. J. Quantum Chem. **S10,** 417 (1976).
[83] B. H. Brandow, Adv. Phys. **26,** 651 (1977).
[84] A. B. Kunz, in: Excited States in Quantum Chemistry, C. A. Nicolaides and D. R. Beck (ed.), D. Reidel Publ. Co., Dordrecht-Boston 1978.
[85] A. B. Kunz, R. S. Weidman, J. Boettger, and G. Cochran, Int. J. Quantum Chem. **S14,** 585 (1980).
[86] A. B. Kunz, J. Phys. C: Solid State Phys. **14,** L455 (1981).
[87] F. Seitz, Modern Theory of Solids, McGraw-Hill, New York 1940.
[88] T. A. Kaplan, P. Horsch, and P. Fulde, Phys. Rev. Letters **49,** 889 (1982).
[89] E. P. Wigner, Trans. Faraday Soc. **34,** 678 (1938).
[90] J. C. Slater, Quantum Theory of Molecules and Solids, Vol. 4, McGraw-Hill, New York 1974.
[91] J. Ladik, in: Electronic Structure of Polymers and Molecular Crystals, J. M. André and J. Ladik (ed.), Plenum Press, New York 1975.
[92] J. C. Slater, Phys. Rev. **82,** 538 (1951).
[93] T. Matsubara and T. Yokota, in: Proc. Int. Conf. Phys., Kyoto-Tokyo 1953.
[94] J. de Cloizeaux, J. Phys. Radium **20,** 606, 751 (1959).
[95] J. B. Goodenough, Phys. Rev. **117,** 1442 (1960).
[96] D. Alder and H. Brooks, Phys. Rev. **155,** 826 (1967).
[97] G. F. Kventsel, Int. J. Quantum Chem. **22,** 825 (1982).
[98] C. Herring, Phys. Rev. **52,** 361, 365 (1937).
[99] M. Lax, Symmetry Principles in Solid State and Molecular Physics, Wiley Interscience, New York 1974.
[100] B. R. Nag, in: Electron Transport in Compound Semiconductors, Springer Series in Solid-State

Sciences, Vol. **11,** M. Cardona, P. Fulde, and H.-J. Queisser (ed.), Springer Verlag, Berlin 1980.
[101] J. C. Slater, Int. J. Quantum Chem. **S3,** 727 (1970).
[102] J. C. Slater, J. B. Mann, T. M. Wilson, and J. H. Wood, Phys. Rev. **184,** 672 (1969); J. C. Slater and J. H. Wood, Int. J. Quantum Chem. **S4,** 3 (1971); J. C. Slater, Adv. Quantum Chem. **6,** 1 (1972).
[103] O. Goscinski, B. T. Pickup, and G. Purvis, Chem. Phys. Letters **22,** (1973); O. Goscinski, M. Hehenberger, B. Roos, and P. Siegbahn, Chem. Phys. Letters **33,** 427 (1975); D. Firsht and B. T. Pickup, Chem. Phys. Letters **56,** 295 (1978).
[104] M. C. Böhm, K. D. Sen, and P. C. Schmidt, Chem. Phys. Letters **78,** 357 (1981); P. C. Schmidt and M. C. Böhm, Ber Bunsenges. Phys. Chem. **87,** 925 (1983).
[105] J. Ladik, Acta Phys. Hung. **23,** 317 (1967); M. J. S. Dewar, J. A. Hashmall, and C. G. Vernier, J. Amer. Soc. **90,** 1953 (1968); P. Čarsky and R. Zahradnik, Top. Curr. Chem. **43,** 1 (1973).
[106] M. C. Böhm, Solid State Commun. **46,** 709 (1983).
[107] M. C. Böhm, phys. stat. sol. (b), in press.
[108] D. S. Boudreaux, R. R. Chance, J. L. Brédas, and R. Silbey, Phys. Rev. **B28,** 6927 (1983).
[109] J. A. Pople and D. L. Beveridge, Approximate Molecular Orbital Theory, McGraw-Hill, New York 1970.
[110] M. Kertész, J. Koller, and A. Ažman, in: Recent Advances in the Quantum Theory of Polymers, Lecture Notes in Physics, Vol. **113,** J. M. André, J. L. Brédas, J. Delhalle, J. Ladik, G. Leroy, and C. Moser (ed.), Springer-Verlag, Berlin 1980.
[111] A. Karpfen, Int. J. Quantum Chem. **19,** 1207 (1981).
[112] D. R. Hartree, The Calculation of Atomic Structure, Wiley Interscience, New York 1957.
[113] R. D. Brown, M. F. O'Dwyer, and K. R. Roby, Theor. Chim. Acta **11,** 1 (1968); R. D. Brown and P. G. Burton, Theor. Chim. Acta **18,** 309 (1970).
[114] M. C. Böhm, Chem. Phys. Letters **89,** 126 (1982).
[115] M. C. Böhm, phys. stat. sol. (b) **121,** 255 (1984); M. C. Böhm, Physical **B 124,** 327 (1984).
[116] M. C. Böhm, unpublished results.
[117] J. Brust, in: Methods in Computational Physics, Vol. **8,** B. Alder, S. Fernbach, and M. Rothenberg (ed.), Academic Press, New York 1968; J. Delhalle, in: Electronic Structure of Polymers and Molecular Crystals, J. M. André and J. Ladik (ed.), Plenum Press, New York 1975.
[118] E. Dubler, M. Textor, H.-R. Oswald, and A. Salzer, Angew. Chem. **86,** 125 (1974); W. Siebert, G. Augustin, R. Full, C. Krüger, and Y.-H. Tsay, Angew. Chem. **87,** 286 (1975); W. Siebert, T. Renk, K. Kinberger, M. Bochmann, and C. Krüger, Angew. Chem. **88,** 850 (1978); W. Siebert, C. Böhle, C. Krüger, and H.-Y. Tsay, Angew. Chem. **90,** 558 (1978); W. Rothermel, C. Böhle, C. Krüger, and D. J. Brauer, Angew. Chem. **91,** 1014 (1979).
[119] L. E. Sutton (ed.), Tables of Interatomic Distances and Configuration in Molecules and Ions, Spec. Publ. No. **18,** The Chemical Society, London 1965.
[120] A. Haaland, Acc. Chem. Res. **12,** 415 (1979).
[121] M. C. Böhm, Z. Naturforsch. **37a,** 1193 (1982).
[122] M. C. Böhm, J. Molec. Struct. (Theochem.) **92,** 73 (1983).
[123] M. C. Böhm, Theor. Chim. Acta **61,** 171 (1982).
[124] M. C. Böhm, J. Chem. Phys. **78,** 7044 (1983).
[125] L. Salem, Acc. Chem. Res. **12,** 87 (1979).
[126] V. Bonačić-Koutecký, J. Čižek, J. Döhnert, and J. Koutecký, J. Chem. Phys. **69,** 1168 (1978); R. Buenker, V. Bonačić-Koutecký, and L. Pogliani, J. Chem. Phys. **73,** 1836 (1980); J. P. Malrieu and G. Trinquier, Theor. Chim. Acta **54,** 59 (1979).
[127] M. Benard and A. Veillard, Chem. Phys. Letters **90,** 160 (1982).
[128] R. S. Mulliken, J. Chem. Phys. **23,** 1833 (1955).
[129] M. Kertész, J. Koller, and A. Ažman, Int. J. Quantum Chem. **18,** 645 (1980).
[130] M. J. Rice and J. Bernasconi, J. Phys. F: Met. Phys. **3,** 55 (1983).
[131] P. Dean, Rev. Mod. Phys. **44,** 127 (1972); R. J. Elliot, J. A. Krummhansl, and P. L. Leath, Rev. Mod. Phys. **46,** 465 (1974); M. Seel, in: Recent Advances in the Quantum Theory of Polymers, Lecture Notes in Physics, Vol. **113,** J. M. André, J. L. Brédas, J. Delhalle, J. Ladik, G. Leroy, and C. Moser (ed.), Springer-Verlag, Berlin 1980.
[132] L. D. Landau and E. M. Lifschitz, Lehrbuch der theoretischen Physik, Vol. **5,** Statistische Physik, Akademie Verlag, Berlin 1975.
[133] R. H. Baughman and G. Moss, J. Chem. Phys. **77,** 6321 (1982); D. Baeriswyl and K. Maki, Phys. Rev. **B28,** 2068 (1983).
[134] P. W. Anderson, in: Amorphous Magnetism, Vol. **II,** R. A. Levy and R. Hasegawa (ed.), Plenum Press, New York 1977.
[135] R. C. Palmer, Adv. Phys. **31,** 669 (1982).